MARITIME TRANSPORTATION RESEARCH AND EDUCATION CENTER
TIER 1 UNIVERSITY TRANSPORTATION CENTER
U.S. DEPARTMENT OF TRANSPORTATION

Maritime Transportation Research & Education Center

The Unintended Consequences of Flood Mitigation along Inland Waterways – A Look at Resilience and Social Vulnerabilities through A Case Study Analysis

July 2020 – March 2023

Janey Camp (PI)
Vanderbilt University
janey.camp@vanderbilt.edu

Jonathan Gilligan (PI)
Vanderbilt University
jonathan.gilligan@vanderbilt.edu

Bowen He
Vanderbilt University
bowen.he@vanderbilt.edu

March 2023

FINAL RESEARCH REPORT
Prepared for:
Maritime Transportation Research and Education Center

ACKNOWLEDGEMENT

This material is based upon work supported by the U.S. Department of Transportation under Grant Award Number 69A3551747130. The work was conducted through the Maritime Transportation Research and Education Center at the University of Arkansas.

DISCLAIMER

The contents of this report reflect the views of the authors, who are responsible for the facts and the accuracy of the information presented herein. This document is disseminated in the interest of information exchange. The report is funded, partially or entirely, by a grant from the U.S. Department of Transportation's University Transportation Centers Program. However, the U.S. Government assumes no liability for the contents or use thereof.

Table of Contents

LIST OF FIGURES

LIST OF TABLES

1. INTRODUCTION

Communities are socio-environmental systems that can be vulnerable to and adversely impacted by natural disasters such as floods, hurricanes, and storms which have long impacted human life and property. Over the past century, efforts have been made to mitigate natural disasters. However, climate-related hazardous losses have progressively increased (Leaning and Guha-Sapir, 2013; He and Ding, 2021; He and Guan, 2021). For example, the United States (U.S.) has lost approximately $17 billion between 2010 and 2018 because of flooding alone (FEMA, 2020). The leading causes of floods are climatic changes, changes in land use, and other anthropogenic activities that include urban growth, deforestation, etc. (Change and Franczyk, 2008). Therefore, building and enhancing community resilience to these disasters and improving natural hazard management strategy are urgently needed to reduce losses in the future and minimize the negative impacts to society (Abrash et al., 2021).

Fluvial and riverine flooding from inland waterways is a primary cause flood damages to communities in the United States. Therefore, considering the mitigation efforts employed along inland waterway communities is critical when considering future resilience. Studies project that due to increasing severity of climate change, riverine flooding along inland waterways will likely increase both in frequency and magnitude in the future (Wobus et al., 2021). Wobus et al., (2021) developed a riverine flood risk model to projection that estimates 20-30% more damages from riverine flooding is likely occur to communities along inland waterways without effective mitigation strategies under the scenario of significant global warming. Thus, acquiring sufficient information and developing computational tools to efficiently evaluate riverine flooding mitigation policies and the potential impacts of those policies on communities such as home buyouts programs are critical.

Additionally, flood vulnerability and risk mapping efforts are focused predominantly on the hydrology and historically have not accounted for consideration of vulnerable populations. Improvements to the approach requires another perspective and changes in the resolution of damage estimates such as those obtained from the US Federal Emergency Management Agency's Hazus (Scawthorn et al. 2006). This requires a granular approach in comparison to historic analysis at a census tract or block level to accurately locate to communities and residents along the inland waterways where riverine flooding usually occurs to estimate and assess the vulnerability and resilience status associated with flood mitigation strategies. One example is found in a study by Messager et al., (2021) which combined fine-scale demographic information interpolated by dasymetric mapping and flood hazard estimation model to reveal the inequities in inland waterways flood vulnerability. The dasymetric mapping in their study accelerated the findings of unequally distributed flood vulnerability that was likely covered by conventional aggregated governmental data (Messager et al., 2021). In another study by Nelson and Camp (2015), d was applied to evaluating flood risks across a community. Thus, novel vulnerability and spatial disaggregation models are two important elements in advancing the current state-of-the-art inland waterways riverine flooding assessment framework.

For years, policies such as those that facilitate home buyout programs have been applied to mitigate hazards impacts after floods (Zavar 2015) in both inland and coastal areas. Home buyouts offer opportunities to flood-affected homeowners that meet certain criteria to relocate to places that are ideally at lower risk of flooding (Fraser et al., 2003). The properties that are bought out are often converted to greenspace to further enhance mitigation of flood impacts and improve community resilience (Nelson and Camp 2020). However, home buyout and other such programs can potentially have unintended consequences in the neighborhoods where they take place. When enough residents relocate out of the community to other places, the social fabric (i.e., a network of interpersonal social connections) and the tax base of the flood affected community can be severely damaged. It has been found that the relocation of community members can cause more socio-economic damages to rural communities than urban communities (Kraan et al., 2021). To date, the adverse impacts of property acquisitions through home buyouts to the social structure of a community is seldomly investigated.

Previous studies have only evaluated the effects of the home buyout program from an individual or household perspective. For instance, Baker et al. (2018) gathered information on the home buyout participants' experience with the acquisition process implemented in their community after Hurricane Sandy in 2012. Nelson and Camp (2020) investigated the economic and environmental benefits of a home buyout program using local data and a series of scenarios for Nashville-Davidson County, Tennessee in the United States. They concluded that proactive implementation is the best approach to remove individuals from harm's way wards the value of benefits compared to other hypothetical scenarios (Nelson and Camp, 2020). McGhee et al., (2020) conducted a survey that used the households that were affected by Hurricane Sandy and participated in home buyouts to measure the change associated with flood hazards risks and social vulnerability. The survey indicated that most households tend to move to places with even higher social vulnerability and higher risks of exposure to coastal flood hazards. This can be due to the challenges of finding equivalent housing in a similar area with the pre-flood market rate offered for homes especially when housing stock is limited post-disaster. Buyout programs may not in fact reduce flood-affected household social vulnerability (McGhee et al., 2020). Studies have also found that home buyout programs may also involve feelings of coercion among the flood-affected population, degradation of trust with other people, and loss of attachment to the places they live (Fraser et al., 2003).

For spatial disaggregation regression models, several previous studies have been proposed to address the spatial non-stationarity challenges in the spatial disaggregation field. For example, Li and Corcoran (2011) suggested dividing the study area into a series of subregions and performing a separate population redistribution within each subregion. The problem with this method is that the strategy of dividing the study area is arbitrary and the rather arbitrary nature of the newly divided subregions' boundaries are unlikely to represent areas with homogeneous population distribution characteristics. Besides, local regression approaches that estimate separate coefficients for each population distribution feature were examined by quantile regression (QR) (Cromley, Hanink, and Bentley, 2012) and geographically weighted regression (GWR) (Lin, Cromley, and Zhang, 2011). Although these approaches advance the traditional global regression method in terms of prediction accuracy, they still did not seem to sufficiently solve the classic problem of the population distribution's heterogeneity and the revealing of the population spatial autocorrelation feature is highly dependent on the configuration of the model's regression covariates and their spatial distribution features (Cockx and Canters, 2015; Lee, 2011). Thus, incorporating spatial autocorrelation in the current dasymetric mapping approach is vital to improve the robustness of the current flood vulnerability assessment framework, especially evaluating community and residents close to the inland waterways where riverine flood usually occur.

In summary, to date, there has not been substantial research conducted on evaluating the effects of a home buyout program on community social fabric. Several research gaps still linger: (1) lack of a means to assess a community's social fabric status which is transferrable and scalable over time and geography (i.e., a social fabric index), (2) lack of a comprehensive assessment framework that can evaluate the validity and the reliability of a community's social fabric index, (3) lack of a reliable spatial disaggregation model to interpolate social indicators into finer spatial scales to avoid the modifiable areal unit problem (MAUP).

1.1 Project Objectives

This project aims to fill such gaps by developing a model for calculating a Social Fabric Index (SoFI) using publicly available data that is both replicable and scalable. To test the model's applicability and robustness, it was applied to a case study area and subjected to uncertainty analysis and global sensitivity analysis. The overall objective of this project is to evaluate the unintended consequences of flood mitigation activities (i.e., buyout programs) represented as community costs of measures such as residential home buyouts. While buyouts are used in both coastal and inland communities as a mitigation approach, this study is focused primarily on a case study of an inland riverine community because an inland community may have more alternatives for mitigation than coastal areas (i.e., relocation and elevation may be more amenable options in some inland areas).

1.2 Scope

This project is focused on developing a Social Fabric Index (SoFI) model whose representative indicators are publicly available that can contribute to the state-of-the-art disaster and social science by addressing the challenge (1) mentioned above. The project has three key parts. In the first phase, we present a literature review of social vulnerability and resiliency indices and use of dasymetric mapping to disaggregate census data and provide more refined considerations for community-level analysis. In the second phase, we develop the SoFI based upon consideration of available data from public sources and the extent to which certain indicators are critical in social fabric analysis. Then, we perform sensitivity analysis to test the robustness of the SoFI model. Finally, the model is then applied to a case study area with geographic information systems (GIS) and other tools used to perform the analysis and create maps demonstrating concepts.

Davidson County, Tennessee, in the United States was utilized as a case study area to study its social fabric and vulnerability (Figure 1). Located in the heart of Tennessee, Davidson County is a primarily urban county spanning over 1300 square kilometers (State and County QuickFacts, 2020). In the 2020 survey, the population was approximately 715,884, with 54.05% being non-Hispanic White (State and County QuickFacts, 2020). One of the most significant natural disasters that has occurred in Nashville was flooding in May 2010. The area was severely affected with more than $2.3 billion in property damages. The home buyout program that has been in use in Nashville for nearly thirty years was carried out as a mitigation strategy to motivate affected people to move to non-affected places aftermath of the 2010 flood, leading to potential heterogeneous influences on the social fabric status across space (Nelson and Camp, 2020). A significant number of homes were bought out prior and after the 2010 flood disaster.

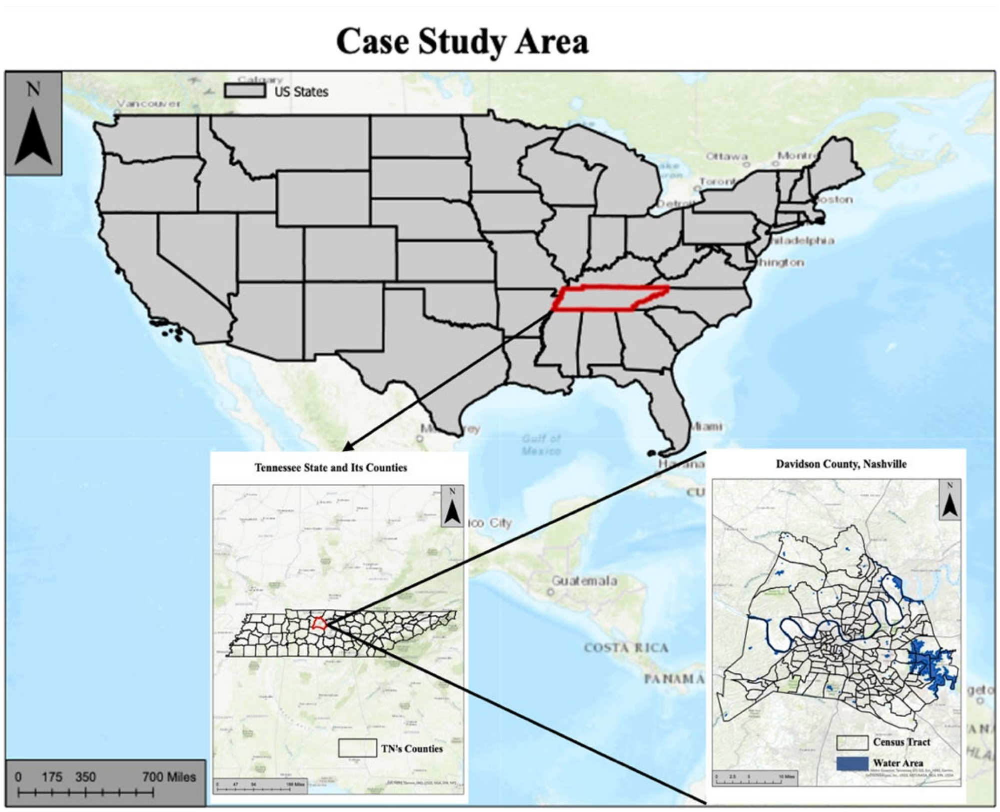

Figure 1. Case study area: the Davidson County, Nashville, Tennessee, U.S.

2. LITERATURE REVIEW

2.1 Community Resiliency and Vulnerability Indices

Resilience and vulnerability are ambiguous and contested concepts (Ford et al. 2018; Meerow and Newell 2019; Cannon and Mueller-Mahn 2010). Both concepts often hold a community's predisaster condition as the reference point for evaluating the impacts of disaster and the goal for recovery, without addressing injustices in that *status quo ante.* Despite these concerns, it can be useful to assess community vulnerability and resilience. Resilience is a socio-environmental system's ability to adapt to external social, political, and environmental disruptions (Adger, 2000). Concerns over growing exposure to natural hazards and lack of community preparedness have stimulated interest in quantitative measurements of resilience (Johansen et al., 2017). Indices are widely used to evaluate resilience and vulnerability because they combine many dimensions of vulnerability or resilience into a single metric, which allows easy assessments of differences across different communities, and of changes over time (Johansen et al., 2017).

Numerous indices of community resilience have been proposed to assess communities and aid in planning (CARRI, 2013; Arup International Development, 2011; Sempier et al., 2010; FEMA, 2008; Plyer, 2013; OSSPAC, 2013). The Community and Regional Resilience Institute (CARRI) quantifies the community's functional capacity to environmental disruptions (CARRI, 2013). The Coastal Resilience Index applies a self-assessment strategy for evaluating historical records and generated resilience indices for each evaluated sector (Sempier et al., 2010). The New Orleans Index uses economic growth, inclusion, quality of life, and sustainability indicators to track the recovery of New Orleans neighborhoods since Hurricane Katrina in 2007 (Plyer et al., 2013). While these resilience measurement approaches provide valuable insights for assessments and planning, many are limited by specificity to geographic areas or types of hazards and lack of explicit quantitative outcomes, which can prevent their generalized application (Johansen et al., 2017). Thus, more work is needed to improve the use of indices to assess community resilience (Johansen et al., 2017).

Similar to resilience, community vulnerability is an ambiguous and contested concept. Here, we define vulnerability as a community's capability to cope, confront, and adapt to the disruptions of a natural disaster (Flanagan et al., 2018). Examples of factors that might affect a community's social vulnerability status include socioeconomic condition, gender composition, race and ethnicity, family structure, education, and medical services (Cutter et al., 2003). Many indices of vulnerability have been created, including: the Social Vulnerability Index (SoVI) to natural hazards (Cutter et al., 2003); the Social Vulnerability Index (SVI) for disaster management (Flanagan et al., 2011); the Environmental Vulnerability Index (EVI) (Kaly et al., 2014); the Coastal City Flood Vulnerability Index (CCFVI) (Balica et al.,2012); and the Human Development Index (HDI) (UNDP, 2016). SoVI is constructed using county-level socioeconomic and demographic data for the U.S. based on 1990 data (Cutter et al. 2003). Using Principal Components Analysis (PCA), an initial set of 42 variables was reduced to 11 independent components, which account for 76 percent of the variance. These components were added together to compute a comprehensive score for each county-the SoVI Social Vulnerability Index. The EVI was constructed using a theoretical framework that identified three aspects of environmental vulnerability: threats to the environment, the innate ability of the environment to cope with the dangers and ecosystem integrity, with the index representing a weighted sum of separate indices of these three aspects of vulnerability (Kaly et al., 2014). The CCFVI assesses vulnerability to coastal flooding, based on exposure, susceptibility, and resilience scores, with the final index representing a weighted sum of hydrological, socio-economic, and political-administrative sub-indices. (Balica et al., 2009, 2012).

Community vulnerability indices provide useful assessment tools that summarizes the multidimensional character of a community's social vulnerability status in a single number. However, reducing a multidimensional portrait of vulnerability to a single index entails normative and political choices of what aspects to emphasize (Gillespie-Marthaler et al., 2019; Ford et al. 2018).

For most of the community resilience and vulnerability indices, the construction process begins with a theoretical analysis, which identifies critical systems that may be affected by disaster or that are expected to play crucial roles in recovery (Gillespie-Marthaler et al. 2019). Next, indicators related to community vulnerability or resilience are selected to represent the identified systems. Such indicators include voter participation (Sherrieb et al., 2010), percent of land used for agriculture (Kaly et al., 2014), and per capita income (Cutter et al. 2003).

Although these indices are constructed using formally similar processes, there are myriad options at each step in the process in which normative judgment is applied, without a disciplinary consensus for identifying and weighting critical systems, selecting indicators, or acquiring and data, and analyzing data to reduce it to a single dimension. This contributes to the confusion and contestation around assessments of vulnerability and resilience (Gillespie-Marthaler et al., 2019; Ford et al. 2018). For instance, some studies identified three critical systems (Pendall et al., 2010), while others identified four (Balica et al., 2009; Norris et al., 2008; Ebisudani and Tokai, 2017; Vita et al., 2018) or even five (Cutter, 2016; Shaw et al., 2010; Tapia et al., 2017; Yoon et al, 2016). Even where the number of categories is the same, their composition can vary significantly. Cutter

(2016) found that ten indicators appeared in 40% of studies, which may provide a starting point for establishing standards, but the 60% of studies that don't include these indicators illustrate the magnitude of the challenge. Gillespie-Marthaler et al. (2019) developed a classification scheme and searching framework to accelerate in identifying, selecting, and applying indicators associated with a variety aspect of social vulnerability. They identified over 550 indicators and metrics of sustainable community resilience, which exhibit similar problems of specification and redundancy.

Another significant challenge for constructing indices lies in the use of correlation analyses to address redundancy among indicators. For a typical index, more than 20 relevant indicators are chosen. Dimension-reduction methods, such as PCA, are used to generate a smaller number of uncorrelated indicators that effectively summarize the original set (Cutter et al., 2003; Cutter et al., 2008; Sherrieb et al., 2010). Using coordinate rotations, such as varimax, with PCA makes the connections between the original indicators and the principal components clearer and easier to interpret (Cutter et al., 2003). However, this analysis framework does not yield a unique index from a set of primary indicators: choices in the analysis procedure can lead to different indices, with different groupings of primary indicators (Cutter et al. 2014; Tapia et al. 2017). Another approach is Confirmatory Factor Analysis (CFA), which was used in the Communities Advancing Resilience Toolkit (CART) (Pfeferbaum et al. 2013, 2015). Shim and Kim (2015) also applied a CFA methodology to integrate a series of resilience dimensions in metropolitan areas of South Korea. Cui and Han (2019) used CFA to assess how well a method developed in Israel (the Conjoint Community Resiliency Assessment Measurement, CCRAM) performed in China. Bec et al. (2019) applied CFA to assess the reliability of an index for measuring resilience to economic structural change in the context of sustainable regional development.

2.2 Global Sensitivity and Uncertainty Analysis on Community Vulnerability and Resilience Indices

The accuracy and reliability of a model's output is critical. Nonetheless, since models are eventually used as an abstraction form to approximate reality, not only the precise input data are rare in the case, but also the modeling process is subject to imprecision, leading to imperfect model output. As a result, the final model product is always associated with certain level of uncertainties and imprecisions which need to be assessed, interpreted, and visualized. Uncertainty and sensitivity analysis are great tools to investigate the imprecisions of the model outputs for user's to be more confident when implementing activities associated with model's results. The difference between the two approaches lie in that uncertainty analysis only evaluates and represents the model outputs' uncertainties, while sensitivity analysis evaluates contributions of the uncertain inputs to the total uncertainties in the model's final outputs.

Uncertainty analysis (UA) is an important process to assess the total possible outcomes associated with their occurrence probability. The goal of uncertainty analysis in models of complex systems is to produce output metrics with a greater degree of confidence, with an underlying aim of improving user's confidences in implementing activities associated with model's output. Uncertainty performance has been widely studied in model predictions of sea level rise (Haasnoot et al., 2020), hurricane paths (Cox et al., 2013), and communities' social vulnerability (Tate, 2013). Two general forms of uncertainty have been well understood: aleatoric and epistemic uncertainty. Aleatoric uncertainty occurs because of the heterogeneity or the intrinsic model randomness. Epistemic uncertainty arises from things that cannot be known but could potentially be measured from the limited accuracy and precision of our measurement (Jakeman, Eldred, and Xiu, 2010).

For example, in terms of social index research, aleatoric uncertainty affects the precision of the input data used for indexes model construction, and epistemic uncertainty affects each step of the model construction process (Tate, 2013). Specifically, epistemic uncertainty could potentially interact with each previous step to generate more uncertainties to the model's output with the development of the index model construction process (Tate, 2013). Uncertainty and sensitivity analysis usually work together to quantitatively validate the social index model where uncertainty analysis focuses on evaluating the robustness of model outputs, and sensitivity analysis assesses the contribution of model's total uncertainty to model's each construction stage.

Different from the uncertainty analysis, sensitivity analysis (SA) focuses on investigating how the model output values respond to model's input changes. While the context where the sensitivity analysis is conducted could be complex, it generally refers to hypothetical scenarios analysis (Pianosi et al., 2016). SA also tells us about how the uncertainties (aleatoric and epistemic) in the independent variables affect the accuracy of our model's predictions of the dependent variables. Sensitivity analysis has been widely studied in human-environmental models such as weather and climate forecasts and simulations (Stephenson and Doblas-Reyes, 2000; Collins et al., 2012), sea level rise (Anthoff et al., 2006), projection of hurricane losses (Iman et al., 2005), evaluation of river water quality (Van Griensven et al., 2002), multizone air flow evaluation (Firrantello et al., 2007) and communities' social vulnerability (Schmidtlein et al, 2008). Besides, studies have also applied the sensitivity analysis to evaluate some uncertain factors associated with model's non-numerical aspects, including model spatial resolution and structure (Baroni and Tarantola, 2014).

Schmidtlein et al. (2008) studied SoVI model's sensitivity to its contexts (Cutter et al., 2003) by considering a series of model uncertainties, including the model spatial scale, indicators selection, geographic contexts, etc. For example, to study the spatial aggregation level factor, they constructed SoVI and applied the principal component analysis (PCA) on three different spatial scales: the county level that was original SoVI scale adopted in Cutter et al. (2003), census tract level scale, and a manually created intermediate level of aggregation (Schmidtlein et al., 2008). They uncovered that the variance explained per principal decreased and the number of principal components selected increased with the decreasing of the level of aggregation at which the principal component analysis was conducted, echoing the result found by Clark and Avery (1976). This is because with increasing level of aggregation, more and more spatial frequencies may be lost, and the same amount of important information can be modelled by fewer numbers of independent variables. In terms of SoVI construction algorithm sensitivity analysis, three index construction stages were incorporated, including PCA selection, PCA rotation, and weighting scheme (Schmidtlein et al., 2008). Within each of the three different categories for index construction, several options were considered. For instance, in terms of PCA component selection, they considered Kaiser criterion, percentage variance explained, Horn's parallel analysis as different methods (Schmidtlein et al., 2008). For PCA rotation methods, they accounted 4 rotation strategies which are unrotated solution, varimax rotation, quartimax rotation, and promax rotation (Schmidtlein et al., 2008). For weighting schemes, three approaches were considered: sum the component scores, first component only, and weighted sum using explainable variance from PCA to weigh each component (Schmidtlein et al., 2008). Factorial analysis with partial ("Type III") sums of squares approach was conducted to assess the model's construction process sensitivity and found that the algorithm is robust to minor changes in variable composition and scale but is sensitive to its quantitative construction stage like weighting scheme (Schmidtlein et al., 2008).

Their sensitivity analysis plays a critical role in understanding the impacts of changes in index construction as well as the scale on the final index representation (Schmidtlein et al., 2008).

Tate (2012, 2013) investigated the uncertainty associated with the methods of SoVI construction process including indicator selection, spatial scale, measurement error, indicator transformation, indicator normalization, and weighting scheme. There are several uncertain alternatives associated with each of these construction stages. For instance, indicator transformation includes three alternatives like raw counts (none), normalized by population (percentage), and normalized by density (area) (Tate, 2013). One of the goals of the uncertainty analysis is to determine if the index model's output is sensitive to the indicator transformation stage. Monte Carlo simulations were applied in the uncertainty analysis process to evaluate uncertainties associated with the SoVI model (Tate, 2013). In the uncertainty measurement and representation stage, three performance statistics to measure the uncertainty magnitude were studied. They are the confidence intervals (CIs), the median rank, and the coefficient of variation (CV). Results showed that for areas with higher vulnerability, there tends to be greater index uncertainty, suggesting that the index model might do a better job at screening low-vulnerability areas rather than accurately identifying high-vulnerability areas (Tate, 2013). They also suggested that it is the weighting scheme that contributes the most uncertainties to the model's output results (Tate, 2013).

2.3 Spatial Disaggregation Approach: The Dasymetric Mapping Analysis

The spatial scale and resolution of interests have been verified by many studies to be important in evaluating the natural disasters' risks and the effectiveness of the mitigation efforts when examining the intersection between natural hazards, mitigation efforts, and community resilience in a multi-level spatial scales (Chakraborty, 2011; Mennis, 2003). The mismatch between spatial units and the actual disaster scales have been verified to affect disaster risk analysis results (Maantay et al., 2007; Mennis, 2002). Especially for the social vulnerability, community resilience, and environmental justice study that heavily rely on the census data from the American Census Survey (ACS), their spatial interpretation of the demographic data in the census tracts (CTs) and census blocks (CBs) are not spatially aligned well with the place of hazard or interest such as the superfund site zones. In addition, the demographic variable such as population, single-person household in a census tract, or a census block spatial is usually too coarse to evaluate the effectiveness of the hazard mitigation efforts. For instance, home buyout activities usually occur in a property or building scale which is much finer than the census tract or block spatial scale. Thus, the spatial scale misalignment problem that occurs in the interface between the real natural hazard and the census boundary zone remains a huge challenge in the current community resilience and natural disaster management research field.

Dasymetric mapping approach has progressed rapidly in recent years because of the development in computation algorithm and Geographic Information System (GIS) (Mennis, 2009; Petrov, 2012). Recently, new innovative ancillary data (e.g. tax parcel data (TP), building footprint data (BDF), and night light data (NTL)) as well as calculation process have received much attentions since they aid in spatially interpolating index-related indicators to a finer spatial scale (e.g. tax parcel or building scale) which is more suitable for environmental justice analyses and hazard mitigation efforts evaluation (Chakraborty, 2011; Bozheva et al., 2005; Eicher and Brewer, 2001; Maantay et al., 2007; Mennis, 2003; Holt and Lu, 2011; Wu et al., 2005). For example, Mennis and Hultgren (2006) invented an intelligent dasymetric mapping (IDM) model that sample on ancillary land cover land use information to determine the relationship between the underlying population surface density and land cover land use type. They also identified the superiority of IDM compared to the traditional areal weighting and 'binary' dasymetric mapping approaches in terms of estimation accuracy (Mennis and Hultgren, 2006). The IDM was widely adopted in the environmental justice and assessment field. For instance, Giordano and Cheever (2010) used IDM to reveal the risk surface from hazardous waste generation in San Antonio, Texas. They found that those socially vulnerable population like Black, or non-homeowners are more likely to be affected by and exposed to risks from the generators. In conclusion, it is the IDM that helped them identify that hazardous waste generation is more likely to affect those socially vulnerable population rather than the general population in Bexar County, Texas (Giordano and Cheever, 2010).

Another important dasymetric mapping technique is the Cadastral-based Expert Dasymetric System (CEDS) (Maantay et al., 2007). Rather than using ancillary information in a uniform spatial resolution such as the land cover data from NLCD that is a 30m resolution, Maantay et al. (2007) developed the CEDS that uses non-uniformly distributed tax parcel information (e.g. property value, property type, and land use information) to delineate the heterogeneity spatial distribution of demographic data such as population in more urban areas such as the New York City (NYC). They conducted an asthma hospitalizations case study in the Bronx, NYC to show the importance of a more accurate population surface product for environmental justice evaluations (Maantay et al., 2007). Nelson et al. (2015) developed a hybrid approach to develop a tax parcel social vulnerability index (SoVI) by linking CEDS method and the SoVI model. The CEDS significantly reveal the underestimated socially vulnerable populations in a finer spatial scale that were masked by original coarser spatial scales (Nelson et al., 2015).

In terms of using the nighttime light (NTL) as an ancillary data, Zhou et al. (2014) adopted the Defense Meteorological Satellite Program/Operational Linescan System (DMSP/OLS) nighttime stable light data (NTL) as ancillary information approximately delineate the urban area. Anther novel dasymetric mapping approach includes using built-area and height data as ancillary data (Alahmadi et al., 2014), using high-resolution address point datasets to conduct the dasymetric mapping (Zandbergen, 2011), creating multi-layer multi-class dasymetric mapping framework to interpolate population distribution (Su et al., 2010), using means of raster pixel maps to rapidly facilitate dasymetric-based population interpolation (Langford, 2007), applying the hybrid model with different ancillary data combination (e.g. land cover data combined with tax parcel data, land cover data combined with NTL) (Briggs et al., 2007; Jia and Gaughan, 2016), and using machine learning model like random forests combined with remotely-sensed and ancillary data to project a finer spatial scale of demographic information distribution (Stevens et al., 2015). Here, we focus on reviewing the IDM and CEDS techniques in this proposal.

The IDM is one of the most popular dasymetric mapping models that consists of a data-driven part and a dasymetric sampling part (Mennis and Hultgren, 2006). The data-driven part of the method applies a land cover land use sampling process to derive the relationship between population surface densities and individual land cover type. It uses the derived density to reallocate the census population data to the land cover finer grids (Mennis and Hultgren, 2006). In their intelligent dasymetric sampling strategy, they developed three sampling methods: the 'containment' method, the 'centroid' method, and the 'percent cover' method (Mennis and Hultgren, 2006). The IDM Toolbox was developed for ArcGIS Pro and can be found at: https://github.com/USEPA/Dasymetric-Toolbox-ArcGISPro.

Cadastral-based dasymetric mapping systems (CEDS) is an important technique for mapping the census data of interest to a finer spatial scale in urban areas (Maantay et al., 2007).

The CEDS method adopts cadastral tax parcel data to redistribute census data to each tax parcel (Maantay et al., 2007). For example, the residential units (RU) and residual area (RA) can be used as population proxy units to derive populations within each tax parcel (Maantay et al., 2007). In many cases, the RA variable misses information in the tax parcel data (Maantay et al., 2007). Thus, they created a new variable, adjusted residential area (ARA) to replace the missing RA variable value (Maantay et al., 2007). By reaggregating the tax parcel level population value to the census block group level, the expert system can determine which proxy unit-number of residential units (RU) or adjusted residential area (ARA) can more accurately interpolate the population surface (Maantay et al., 2007). Then, the expert system would select the optimal proxy to perform the spatial disaggregation task (Maantay et al., 2007). However, the disadvantage of this method is that its applicability is restricted by the tax parcel data availability of the study area of interest.

3. METHODOLOGICAL APPROACH

3.1 Social Fabric Index (SoFI) Model

The term "social fabric" refers to the degree of interpersonal connection and cohesion, and connection to place among community members. It embraces numerous interrelated phenomena, including demographic and economic factors, behavioral issues, social structures, social organizations, social networks, and relationships among people (Tanner et al., 2020). Different sociological perspectives profoundly influence the concept of social fabric and its operationalization in a specific analysis method. Civil society and social fabric describe the ability of a geographic place "to nurture local spaces, facilitate micro-organizations and support the multiplicity of cultural matrixes comprising civil society" (Cruz et al. 2009).

In this project, we present a method for constructing a community Social Fabric Index that includes only physical or behavioral aspects of community rather than their emotional effects. This decision makes it easy to apply the method using widely available public data, without requiring difficult and expensive surveys of community members and their attitudes. We use metrics such as the number of churches and the amount of green, public spaces as proxies for attachment to place.

In summary, we capture the social cohesion and fabric from the following perspectives:

(1) Sociodemographic and economic factors, such as population and gender.
(2) Social institutions, such as family structure and composition.
(3) Social organizations, such as voluntary-based groups and churches.
(4) Social networks or relationships among people, such as community-wide events.
(5) A sense of belonging and identification with a particular social unit.
(6) A sense of social justice and equity, particularly in government policies, such as public hearings and elections.
(7) A willingness to participate in shared activities and possibly undertake voluntary work.
(8) A sense of life satisfaction, happiness, and positive future expectations.
(9) A sense of safety and security, such as fire stations, and emergency rooms.

Different from traditional Social Vulnerability Index model (SoVI) (Cutter et al., 2003) which mainly includes standard sociodemographic data from American Community Survey, the proposed SoFI model incorporates several new dimensions including the community cohesion and engagement, social organization, public facilities, and amenities that take people's relationship and connectivity within a community into consideration (Figure 2).

Many studies have identified a strong association between sociodemographic diversity and social cohesion. Recent studies find that ethnic heterogeneity strengthen social fabric, by promoting greater trust among members with different ethnic features (van der Meer and Tolsma 2014) and refute older studies which claimed that social capital and cohesion can be weakened by ethnic diversity (Putnam 2007). Thus, we included several ethnic indicators, such as the percentage of Asian, Hispanic, and Black populations in the model. Education strengthens social cohesion by enabling new members to be engaged in the social connections (Kantzara, 2011). Additionally, education also promotes healthy lifestyles and social norms, reducing social inequalities (Kyllönen, 2019). Thus, the percentage of population with limited education was included in the model. Religion is another source of social cohesion, through its role in strengthening shared values, sense of attachment, as well as fostering a sense of belonging (Zhang et al., 2019). Nonetheless, data on religious affiliation is not generally accessible, and its spatial distribution is not measured consistently in extant surveys (Miller 2016); therefore, we use the number of religion-related buildings as its approximations.

Relationships between families play important roles in community cohesion (Ravanera, 2000), and children are especially important to building inter-family connections in a neighborhood, at school, and in the greater community (Beaujot, 2000). For many adults, retirement precipitates a changing relationship with the community (Ravanera, 2000). In the past, adults who spent much of their adult life in the labor force, and their spouses, benefitted from pensions and other accumulated resources that can meet their needs in retirement and allow for informal and formal charitable giving (Ravanera, 2000). Retireees also have more time for volunteering formally or informally within the community (Ravanera, 2000). Thus, households with seniors are also good potentials to strengthen community cohesion and fabric. However, this may change as the majority of a new generation of retirees has not had access to defined-benefit pensions, and has not been able to save adequately for retirement (Ellis et al. 2014). While recognizing the shortcomings of a focus on families, we nonetheless include demographic statistics on the fraction of single-parent and single-adult households, as these have been found to correlate negatively with social cohesion (Fukuyama, 1995). Financial burdens, such as high cost of housing relative to household income, can discourage formation of new families (Wrenn et al., 2019; Hu et al., 2021). Thus, the proportion of single-parent and single-adult households may reflect social cohesion of a community, both through the direct contribution of families to social cohesion, and as an indirect measure of the economic health of the community (Kim and Kim, 2020; Beaujot, 2000; Tanner et al., 2020).

Community engagement and place of attachment are also core elements in promoting community identity and strengthening the social and cultural fabric (Manzo and Perkins, 2006). In a cohesive and engaged community, people not only like to be surrounded by each other, but also has a strong place attachment feeling to the place in which they live in and never want to leave. They are willing to participate in community public events like festival gatherings to hold aspirations for improving the community's common good (Adha et al., 2018). Study found that social cohesion can be significantly improved by engaging public organizations' work into social system (Andrews, 2014). Residents are willing to participate in responsive development of community from economic and social perspective since they have a strong belief that they can possess their own future. A cohesive community also shares a common vision and a sense of belonging with each of its member. One significance is that it greatly appreciates and values the opinions and thoughts from people with very different backgrounds (Local Government Association, 2002). Participation in public affairs is particularly productive in enhancing community cohesion and engagement since people with variety interests have a chance to reach an equilibrium so that the whole community can be seen as one interest entity (Cantle, 2001). Thus, we included several indicators associated with community public affairs engagement, activities, such as the number of community events, elections, and hearings as indicators in the model.

Community events include the initiatives of public socials by an HOA or an apartment property management team in that all neighboring residents can participate to know each other better. Community elections include elections of volunteer representative residents for an HOA board by fellow neighbors. Community hearings are gatherings and events held by officials and residents, in which residents are permitted to comment on public or political issues before the actions are taken. One example is the metro council meetings held by the Nashville city government in the David Scobey Council Chambers at the Historic Metro Courthouse located at One Public Square. Any public members wishing to speak at a public hearing can attend and express opinions.

The level of reported crime in disadvantaged areas is related to low levels of social cohesion (Hirschfield and Bowers, 1997). Study identified that for those areas with high levels of social cohesion, crime rates are significantly lower than expected compared to those areas with low levels of social cohesion (Hirschfield and Bowers, 1997). This correlation may be explained by the fact that social cohesion plays a critical role in reducing crime rates for a community (Sampson et al. 1997; Dominguez & Montolio 2021).

However, collecting data on people's perception of community cohesion and attachment to place is challenging and time consuming without conducting large scale community surveys. Fortunately, important connections have been observed between the place attachment and the practice of community participation and the planning process (Manzo and Perkins, 2006). Thus, we used non-residential historical site like monuments as a proxy to approximate place attachment (Carpenter, 2013). It is believed that people who are associated with stronger feelings of place attachment and are more motivated in participating community public affairs (Carpenter, 2013).

Public facilities and amenities are essential in enhancing residents' social values by providing physical spaces for interaction and integration (Latham and Layton, 2019; Yuliastuti, 2018). Thus, it is considered a valuable aspect of the social fabric of a community. The study found that people connect to a community through their physical built environment and the assets that the environment affords them (Tanner et al., 2020). The economic and social aspects of these infrastructures facilitate social connection, participation, integration, and improve social connectivity positively and negatively (Tanner et al., 2020). For example, schools serve as a physical medium where residents can communicate, help, and educate others. Restaurants and cafes provide valuable spaces for people to have meals together with their friends. They create more opportunities for people to have meals together and exchange opinions on cuisines and cultures, strengthening the social ties between individuals. As a result, in a community with sufficient public facilities, people can feel safe, secure, connected, and happy. We included a series of facilities and amenities, like the number of green spaces, barbers, supermarkets, universities, and fire stations, as indicators to reflect a community's capability to provide opportunities for its residents to exchange physical and spiritual resources in a common shared space.

The relationship between economic prosperity and the community social fabric can be substantial (Tanner et al., 2020). Studies showed that people associate affluence with strong social ties (Tanner et al., 2020). For example, people always want to go to communities with affluent choices of shopping centers, and public green spaces that require the community's economic investment. People tend to believe that economic prosperity are essential for a strong social cohesive community to thrive (Tanner et al., 2020). Meanwhile, a high-quality economy also facilities the prosperity of local businesses such as pubs and restaurants so that people have more places to consume and interact with each other. This could readily lead to a virtuous circle in that a stronger economic strengthens the local tax base, thus enabling the potential of more public facilities investment to further allure more population to move in. Ideally, we want to describe a community's economy status from five perspectives: revenue, debt, investment, tax, and GDP. The revenue is the per capital monetary income of all people and local businesses within a community. The debt is the per capital debt of all people and local businesses within a community. The investment is the per capital financial investment from all people and businesses outside a community. The tax is the per capital monetary tax contributed by all people and businesses within a community. The GDP is the per capital gross domestic product of a community. However, since this information is tough to obtain from a public data source, we included some indicators that are publicly accessible to approximate the financial status of a community, like median gross income, unemployment rate, median gross rent, median house value, and the number of cafes/pubs per capita.

Voluntary, publicly supportive organizations are believed to have significant impact on societal levels of social cohesion (Heuser, 2005). Relevant studies suggested that active participation in voluntary and supportive organizations often lead to autonomous actions that are shaped and carried out for the common good (Heuser, 2005). Fukuyama (1995) pointed out that the satisfaction we derive from being connected to others grows out of a fundamental desire for recognition. Active participation in a voluntary organization involves our need for human connectedness. The voluntary and supportive organizations can include national and international nonprofit/nongovernmental organizations (NGOs), places of worship, unions and lobbies, and a wide array of special interest groups. Although their respective functions, sizes, structures, and missions can vary greatly, every one of them purports to bring people together who share similar ideals to achieve common goals (Heuser, 2005; Woolley, 2016). Given the limited options for data that designates such gathering places, we calculated the number of churches, cathedral buildings, chapels, mosques, charities, temples, etc. (i.e., places of worship) as indicators to approximate the voluntary and supportive organizations.

Based on the literature above, seven critical dimensions associated with community social fabric status were identified, and their corresponding indicators are displayed in Figure 2. Dimension and related indicators description are summarized in Table 1. These indicators were incorporated in the proposed SoFI. Data was derived from the American Community Survey (ACS). For example, gender diversity was derived by calculating the difference between the male and female population, and ethnic diversity was approximated by calculating the standard deviation of the ethnic group populations. For the identified public facilities and amenities indicators, data was manually derived from GoogleMaps, state registered charities search engines, governmental crime activity maps, and the Open Street Map data source. Some of the social organization, community relationships, and community cohesion and engagement indicators, were approximated by relevant physical facility indicators.

After the selected indicators were collected, SoFI was constructed based on an inductive configuration since it begins with a large set of indicators (Tate, 2012). Options for each of the model's construction stages were arbitrarily selected to serve as a baseline. We use italics in Table 2 to show the baseline options for each construction stage. Specifically, all selected indicators were normalized based on the corresponding census tract unit area and standardized using z-score standardization. Then, principal components analysis (PCA) was performed on the normalized and standardized indicators. Following this, the Kaiser criterion was adopted for principal component selection, and varimax rotation was adopted for principal component interpretation. Finally, a new summary index named "SoFI" was calculated by directly summing all the selected principal components based on Kaiser selection and varimax rotation interpretation results. All calculations were implemented in the RStudio software. Then, the calculated data was exported to ArcGIS Pro to visualize the spatial distribution of the social fabric index.

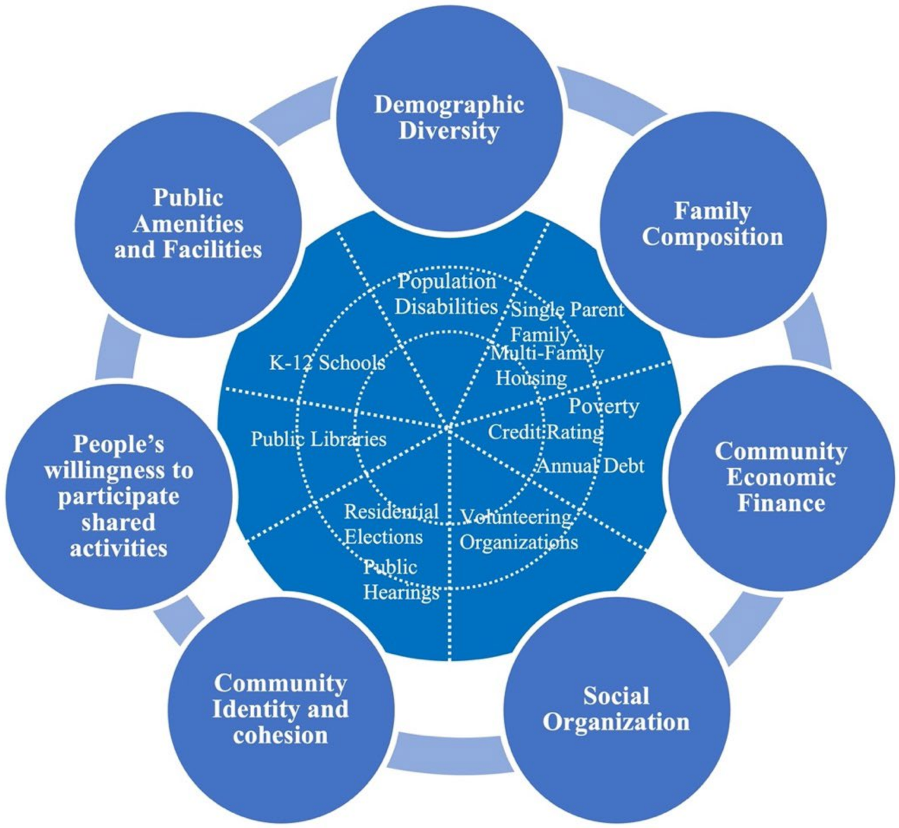

Figure 2. Scoping diagram for communities' social fabric dimensions.

Table 1. Social Fabric Dimension and Indicators

Dimension	Description	Indicators
Sociodemographic Diversity	Differences among people in various forms including gender, ethnic, education attainment, etc. ***Sources:*** MacDonald and Sampson (2012), Monteil et al. (2020), van der Meer and Tolsma (2014), Putnam (2007), Kantzara (2011), Kyllönen (2019)	POP, MALE_POP, FEMALE_POP, ASIAN, RELIGIOUS_POP*, BLACK, HISPANIC, WHITE, LIMIT_EDUCATION, LIMIT_ENGLISH
Community Cohesion and Engagement	Community people's participation in public policy affairs. ***Sources:*** Cortes Jr (1997), Tanner et al. (2020), Adha et al. (2018), Andrews (2014), Carpenter (2013), Hirschfield and Bowers (1997), Cantle (2001), Manzo and Perkins (2006)	COMMU_EVENT*, COMMU_ELECTION*, COMMU_HEARING*, CRIME

Community Economy/Finances	Community's monetary and economic values ***Sources:*** Tanner et al. (2020)	COMMU_REVENUE*, COMMU_DEBT*, COMMU_INVEST*, COMMU_GDP*, COMMU_TAX*, MEDIAN_INCOME, UNEMPLOYMENT, POVERTY, MEDIAN_HOUSE_VALUE, MEDIAN_GROSS_RENT
Family Composition/Structure	Differences among family structure within a community including single parent family, married couple family, etc. ***Sources:*** Nickols et al. (2015), Zahda and Fukukawa (2008), Ahlbrandt (2013)	FAM_OWN_CHILD, SING_PARENT_FAM, SING_PERSON_HOSHD, MULTI_FAM_HOUS, SENIOR_HOUS, TOT_HOUSHD
Social Organization	The community-led non-profit organizations that can provide public and voluntary services to its people. ***Sources:*** Woolley (2016), Heuser (2005), Fukuyama (1995)	SUP_GRP*, VOL_GRP*, CATHEDRAL, CHAPEL, MONSTERY, MOSQUE, RELIGION, TEMPLE, CHURCH, CHARITY
People's willingness to participate in shared activities (Relationships)	The public places density that enables people to participate shared activities to enhance their connections. ***Sources:*** Corcoran et al (2008), Gallent et al. (2003), Tanner et al. (2020)	RECREATION, PUB, MONUMENT, STADIUM, CAFÉ, RESTAURANT
Public Amenities and Facilities	The public physical amenities that create opportunities to nurture and organize people within a community. ***Sources:*** Carpenter (2013), Latham and Layton (2019), Yuliastuti (2018),	FIRE_STATION, GROCERY, SUPERMARKET, EMERGENCY, HEALTHCARE, HOSPITALS, COLLEGE, KINDERGARTEN, LIBRARY, K-12_SCH, PUBLIC_SCH, PRIVATE_SCH, UNIVERSITY, BANK, BUS_STOP, GREEN, BARBER

3.2 Global Sensitivity and Uncertainty Analysis on the SoFI Model

There are two general forms of uncertainty associated with models, including aleatoric and epistemic. Aleatoric is caused by model's heterogeneity and the inherent randomness of input parameters and processes (Kiureghian and Ditlevsen, 2009). The epistemic uncertainty is caused by an incomplete and imprecise understanding of model parameters (Helton et al., 2010).

Traditionally, every stage of the SoVI construction step is arbitrarily selected, ignoring any epistemic uncertainties that accompany every step of the index construction process. However, epistemic uncertainty could interact with previous steps and propagate with the proceed of modeling decisions during the index development process.

Thus, this project performed an uncertainty and global sensitivity analysis on the SoFI model to answer the following research questions: (a) How much uncertainty is associated with the SoFI model? (b) How is the SoFI model connected to uncertainty? (c) Which modeling decision contributes the most to uncertainty in the SoFI model? To address these questions, model options for an inductive SoFI for Davidson County, Nashville, were subjected to an uncertainty analysis and variance-based global sensitivity analysis approach. The uncertain model decisions evaluated are summarized in Figure 3.

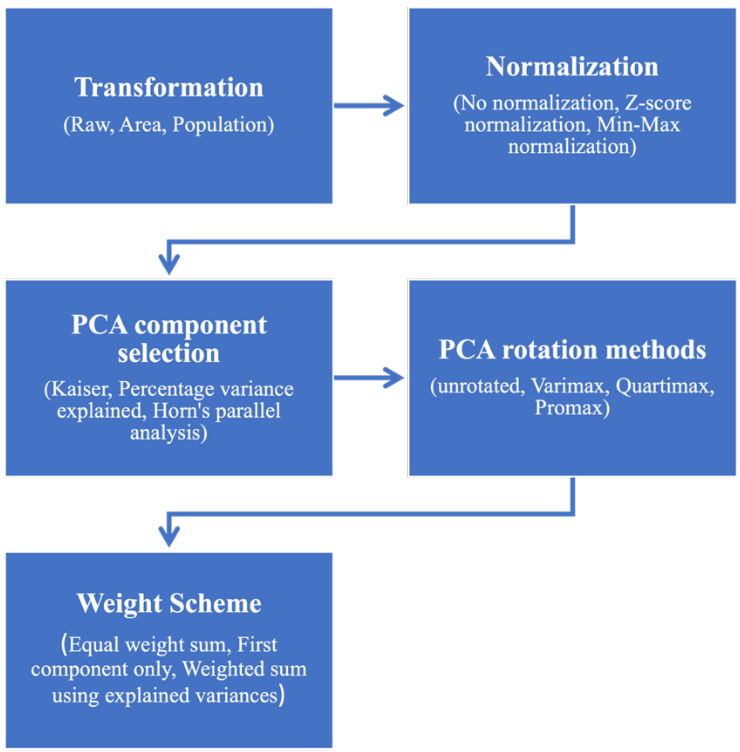

Figure 3. Diagram of uncertain construction factors associated with social fabric index (SoFI) composition process.

Table 2. Uncertainty analysis model factors.

Construction stage	Options	Probability density function
Indicator transformation	Raw Data *Averaged by area* Averaged by population	Discrete (1, 2, 3)
Indicator normalization	Raw Data *Z-score normalization* Min-Max normalization	Discrete (4, 5, 6)
PCA component selection	*Kaiser selection* Percentage variance explained Horn's Parallel analysis	Discrete (7, 8, 9)
PCA rotation methods	Unrotated	Discrete (10, 11, 12, 13, 14, 15)

	Varimax rotation Quartimax rotation Promax rotation (m = 2, 3, 4)	
Weight scheme	*Equal weight sum* First component only Weight sum using explained variances	Discrete (16, 17, 18)

Indicator Transformation

1. Raw data: no transformation method is applied.
2. Averaged by area: every indicator values are divided by the corresponding spatial unit area.
3. Averaged by population: every indicator values are divided by the corresponding total population.

Indicator Normalization

1. Raw data: no normalization method is applied.
2. Z-score normalization: z score is calculated based on $z = \frac{x-\mu}{\sigma}$, where x is the individual indicator value, μ and σ are the mean and standard deviation of that indicator, respectively.
3. Min-Max normalization: minimum value gets transformed into 0 and maximum value get transformed into 1: $x' = \frac{x - \min(x)}{\max(x) - \min(x)}$

PCA Component Selection

1. Kaiser criterion (Kaiser, 1960): principal components whose eigenvalues are greater than one are valid to be selected.
2. Percentage variance explained: select principal components to explain an 80% amount of variation in the original data.
3. Horn's parallel analysis (Horn, 1958): retain principal components whose eigenvalues are larger than the expectation value by randomly generating 100 data sets.

PCA Rotation Methods

1. Unrotated solution: no rotation is applied.
2. Varimax rotation (Kaiser, 1958): load each variable highly on just one component.
3. Quartimax rotation (Neuhaus, 1954; Carroll, 1953; Ferguson, 1954; Saunders, 1953): enlarge the difference between large and small loadings, so that each variable loads only a few principal components.
4. Promax rotation (Hendrickson & White, 1964): this method adopts an oblique rotation that make principal no longer orthogonal. A power parameter must be specified in this method, in this project, values of 2, 3, and 4 were selected for this rotation algorithm.

Weight Scheme

1. Equal weight sum: a simple approach to sum up all the selected principals.
2. First component only: only select the first principal component to compose the SoFI.
3. Weighted sum using explainable variance: each principal component is weighted based on the proportion of total variation that the principal component explains and then sums together to get the summary score.

Variance-based Global Sensitivity Analysis

Variance-based global sensitivity analysis is the most appropriate method for assessing non-linear mathematical models, such as the index composite model (Saltelli, Tarantola and Campolongo, 2000). A sensitivity index can be developed to measure the sensitivity of a given input factor X_i (X_i is the modeling factors include transformation, normalization, PCA computation methods, and weighting scheme) by computing the fractional contribution to the model output variance due to the uncertainty in X_i (Saltelli et al., 2004). Formula (1) represents the calculation of sensitivity indices for a model with k independent input factors. For a model of the form $Y = f(X_1, X_2, \dots X_k)$, the total output variance $V(Y)$ of the model output Y (Saltelli et al., 2004) is:

$$V(Y) = \sum_i V_i + \sum_i \sum_{j>i} V_{ij} + \cdots + V_{12\dots k} \tag{1}$$

The total variances of the model output Y can be decomposed by each input factor's contribution to the total model output variance V_i and all interactions of these V_{ij} could term up to the order of k for a model with k uncertain input factors.

where

$$V_i = V_{X_i}\{E_{\boldsymbol{X}_{-i}}(Y|X_i)\} \tag{2}$$

X_i is the i-th input factor and $\boldsymbol{X_{-i}}$ denotes the matrix of all input factors but X_i. The inner expectation operator is that the mean of Y is taken over all possible values of $\boldsymbol{X_{-i}}$ while keeping X_i fixed. The outer variance is taken over all possible values of X_i. Thus, the interactive effects between input factors i and j can be derived:

$$V_{ij} = V_{X_i X_j}\left\{E_{X_{-ij}}(Y|X_i, X_j)\right\} - V_{X_i}\{E_{X_{-i}}(Y|X_i)\} - V_{X_j}\{E_{X_{-j}}(Y|X_j)\} \tag{3}$$

Based on the law of total variance:

$$V_y = V_{X_i}\{E_{X_{-i}}(Y|X_i)\} + E_{X_i}\{V_{X_{-i}}(Y|X_i)\} \tag{4}$$

The first order sensitivity index is computed as the fraction of the unconditional output variance $V(Y)$ that is contributed by the uncertainty in X_i (Saltelli et al., 2004):

$$S_i = V_i/V(Y) \tag{5}$$

For a linear model, $\sum_{i=1}^{k} S_i = 1$ and the first-order conditional variances of equation (1) are sufficient to the model's total output variance. Nonetheless, for a non-linear model, higher-order sensitivity indices, which are responsible for interaction effects among sets of input factors, need to be computed. For a model with k independent input factors, the total number of indices (including $S_i s$) that should be estimated is as high as $2^k - 1$. Thus, we calculate a second order of the sensitivity index that incorporates all the interactions involving a given factor X_i as S_{Ti} (Saisana et al., 2005, Homma and Saltelli, 1996, Saltelli et al., 2004):

$$S_{Ti} = 1 - \frac{V_{X_{-i}}\{E_{X_i}(Y|X_{-i})\}}{V(Y)} \tag{6}$$

where $V_{X_{-i}}\{E_{X_i}(Y|X_{-i})\}$ is considered as the first order variance contributions of all factors but X_i. Thus, $V(Y) - V_{X_{-i}}\{E_{X_i}(Y|X_{-i})\}$ must give the contribution of all terms in the variance decomposition that do include X_i, which is recognized as total order variance contributions.

If there are interactions exist between the model input factors, $\sum_{i=1}^{k} S_{Ti} > 1$. For any given factor X_i, a significant difference between S_i and S_{Ti} indicates that interactions between factors are vital. Identifying factors' interactive effects enable us to understand better of the non-linearity of the model structure (Saisana et al., 2005).

Here, we also discuss the existing estimators and approaches to compute both sets of sensitivity indices S_i and S_{Ti} from a single set of simulation, which is the computation of an individual value of model output Y mapped from a sampled set of k factors $X_1, X_2, \dots, X_k$. Supposed we have two independent sampling matrices **A** and **B** for simulating *N* experiments for a model with k input factors, with a_{vi} and b_{vi} as their generic elements. The column index *i* indicates the input factors, which runs from one to *k*, and the row index v contains the simulation samples, which runs from one to *N*. To introduce variabilities of input factors, the matrix $\mathbf{A}_{\mathrm{B}}^{(i)}$ is constructed where all columns are from **A** except the *i*-th column which is from **B**. Thus, all that is needed to compute both sets of S_i and S_{Ti} for the k factor-model is the triplet of matrices **A**, **B**, $\mathbf{A}_{\mathrm{B}}^{(i)}$**.** Table 3 shows an example of a set of **A**, **B**, $\mathbf{A}_{\mathbf{B}}^{(i)}$ triplet matrices with *N* = 5 simulation realizations.

Table 3. Example of a set of **A, B,** $\mathbf{A}_{\mathbf{B}}^{(i)}$ triplet matrices with *N* = 5 simulation realizations.

A						**B**					
	1	**4**	**7**	**10**	**16**		**1**	**4**	**7**	**11**	**16**
	2	**4**	**7**	**10**	**16**		**1**	**4**	**7**	**10**	**16**
Q	**1**	**5**	**8**	**11**	**17**	**Q**	**1**	**5**	**7**	**10**	**17**
	3	**5**	**7**	**11**	**17**		**1**	**5**	**8**	**11**	**16**
	1	**6**	**7**	**11**	**16**		**2**	**4**	**9**	**10**	**18**
	1	**4**	**7**	**10**	**16**		**1**	**4**	**7**	**10**	**16**
	1	**4**	**7**	**10**	**16**		**2**	**4**	**7**	**10**	**16**
$\mathbf{A}_{\mathbf{B}}^{(1)}$	**1**	**5**	**8**	**11**	**17**	$\mathbf{A}_{\mathbf{B}}^{(2)}$	**1**	**5**	**8**	**11**	**17**
	1	**5**	**7**	**11**	**17**		**3**	**5**	**7**	**11**	**17**
	2	**6**	**7**	**11**	**16**		**1**	**4**	**7**	**11**	**16**
....											

Here, the estimator of Saltelli et al. (2010) was adopted to calculate the first order of the sensitivity index S_i:

$$S_i = \frac{\frac{1}{N}\sum_{v=1}^{N} f(\boldsymbol{B})_v [f(\boldsymbol{A}_B^{(i)})_v - f(\boldsymbol{A})_v]}{V(y)} \tag{7}$$

please see Saltelli et al. (2010) for more detailed mathematical derivation.

The method of Jansen (1999) was used to calculate the total order of sensitivity index S_{Ti}, following the best practices identified by recent studies (Saltelli et al. 2010; Puy et al., 2020):

$$S_{Ti} = \frac{\frac{1}{2N}\sum_{v=1}^{N}[f(\boldsymbol{A})_v - f\left(\boldsymbol{A}_B^{(i)}\right)_v]^2}{V(y)} \quad (8)$$

where any sampling point in either **A** or **B** sampling matrix can be indicated as x_{vi}, where v and i respectively index the row and the column. Please see Jansen (1999) for more detailed mathematical derivation. Estimators for both S_i and S_{Ti} were reviewed in Chan et al. (2000).

Sobol's (1967) method of Quasi-Random sampling was used as the sampling algorithm for selecting the input factors. To compute the pair (S_i, S_{Ti}) values, 2*N* simulation are ran for model output Y corresponding to matrices **A**, **B**, while *kN* simulations are ran to compute Y from $\mathbf{A}_\mathbf{B}^{(i)}$. Thus, the sensitivity indices pair can provide good approximation to the model sensitivities at a reasonable cost with a $N(k + 2)$ model samples, where N represents the sample size of **A** or **B** matrices (Saisana et al., 2005). N typically varies in the 100 -1000 range. All the sensitivity computation processes were conducted in the R package sensobol (Puy et al., 2021). The detailed experiment design is summarized in Table 4.

Table 4. Experiment design of uncertainty and sensitivity analysis.

	Uncertainty Analysis		**Sensitivity Analysis**
N	2^9	**Estimator**	First order: "saltelli", Saltelli et al. (2010)
K	5		Total order: "jansen", Jansen (1999)
Model evaluation	$N(k+2)$ = $(5+2) \times 2^9 = 3584$	**Matrices**	c ("**A**", "**B**", "$\mathbf{A}_\mathrm{B}^{(i)}$")
Input Factor PDF	Uniform Discrete	**Sample Algorithm**	Quasi-Random sampling

3.3 Dasymetric Mapping: A Hierarchical Poisson Spatial Disaggregation Regression Model (HPSDRM)

The hierarchical Poisson spatial disaggregation regression model in the context of population dasymetric mapping is proposed as follows. Suppose $\mathcal{A} \in \mathbb{R}^2$ denotes the study area of the interest that can be partitioned into $n_\mathcal{A}$ areal units $\mathcal{A}_1, \ldots, \mathcal{A}_{n_\mathcal{A}}$ and $Y_{\mathcal{A}_1}, \ldots, Y_{n_\mathcal{A}}$ are their corresponding areal population observations. Suppose Y_i denotes the number of persons at a grid point s_i within area $\mathcal{A}_i$ that is unobserved. The purpose is to interpolate the quantity of interest Y_i over a set of finer n_p grid points $s_1, \ldots, s_{n_p}$ from $n_\mathcal{A}$ coarser areal observations. Two levels of spatial random effects are incorporated to characterize the spatial autocorrelation features at both grids and the areal levels. The proposed population HPSDRM is characterized by a Poisson Regression Model for the target grid and observed area value:

$$Y_i \sim Poisson(\mu_i),\ i = 1, \ldots, n_p \quad (9)$$

$$\mu_i(\gamma) = exp(\gamma),\ i = 1, \ldots, n_p \quad (10)$$

where the linear predictor γ for grids level with spatial random effects is characterized as follows

$$\gamma_i = \boldsymbol{x}_i'\boldsymbol{\beta} + \eta(s_i) + \phi_{\mathcal{A}_i},\ i = 1, \ldots, n_p \quad (11)$$

$\boldsymbol{x}_i'$ are $k \times 1$ vectors of selected land cover covariates for the ith grid point and $\boldsymbol{\beta}$ is the corresponding regression coefficients vector. Here, the link function is a log function, which is common for modeling counts data. The spatial noise is modeled as two sets which are all realizations of Gaussian random processes. The first set of spatial random effects $\boldsymbol{\eta} = (\eta(s_1), \dots, \eta(s_{n_p}))$ characterize grid level's spatial autocorrelation that assumes the population in closer grids is more similar than that in grids far apart. These random effects are assumed to be a zero-mean stationary gaussian random field, that is $\eta \sim N(\boldsymbol{0}, \Sigma)$, where Σ is a Matérn kernel such that for generic grid point s_x and $s_y \in \mathbb{R}^2$, we have

$$\Sigma_{xy} = Cov\left(\eta(s_x),\, \eta(s_y)\right) = \frac{\sigma_\eta^2}{2^{\nu-1}\Gamma(\nu)}\left(\kappa\|s_x - s_y\|\right)^{\nu} K_\nu(\kappa\|s_x - s_y\|) \tag{12}$$

where $\|\cdot\|$ denotes the Euclidean distance between the spatial grid point s_x and s_y, σ_η^2 is the marginal variance of the process, κ is a scaling parameter that controls the range $r(r = \frac{\sqrt{8\upsilon}}{\kappa})$ which is the distance where spatial correlation is approximately 0.1 (Matérn, 1986). K_ν is the modified Bessel function of the second kind, and ν is the smoothness parameter that is often set as a constant due to identifiability issues (Abramowitz and Stegun, 1972). Here, we set $\nu = 1$ based on Lindgren et al. (2011).

The second set of areal level spatial random effects $\boldsymbol{\phi} = (\phi_1, \dots, \phi_{n_\mathcal{A}})$ characterizes observed areal data's spatial autocorrelation and can be modeled by a conditional autoregressive (CAR) prior. We apply the CAR model proposed by Leroux et al. (2000), which was identified as the best models in recent studies (Lee, 2011, Utazi et al., 2019). These spatial random effects are also assumed to follow a zero-mean gaussian random process that $\phi \sim N(\boldsymbol{0}, \sigma_\phi^2 \boldsymbol{Q}^{-1}(\boldsymbol{W}))$, where $\boldsymbol{Q}(\cdot)_{n_\mathcal{A} \times n_\mathcal{A}}$ is a precision matrix and σ_ϕ^2 is the marginal variance parameter of the gaussian process. Specifically, $\boldsymbol{Q}(\boldsymbol{W}) = \rho(\mathrm{diag}(\boldsymbol{W}\boldsymbol{1}) - \boldsymbol{W}) + (1 - \rho)\boldsymbol{I}_{n_\mathcal{A}}$, where ρ is a spatial autocorrelation mixing parameter, $\boldsymbol{1}$ is an $n_\mathcal{A}$ vector of 1's, $\boldsymbol{I}_{n_\mathcal{A}}$ is the identity matrix and $\boldsymbol{W}$ is a binary matrix capturing the neighborhood information of the areas. For which $W_{ij} = 1$ if areas $\mathcal{A}_i$ and $\mathcal{A}_j$ are neighbors to each other and $W_{ij} = 0$ otherwise. The neighboring areas are defined in a contiguous context that they share at least one vertex. $\phi_{\mathcal{A}_i}$ is the spatial random effect of the area $\mathcal{A}_i$ that the ith grid belongs to.

These spatial noise terms can be thought of as random effects influencing population distribution but cannot be measured by observations. The population counts observed in tract j, Y_j, is assumed to be the sum of all the unobserved counts of population in each grid i inside the tract j.

$$Y_j = \sum_{i=1}^{N_j} y_i \tag{13}$$

where Y_j is the observed population count in the tract j, N_j is the number of grids inside the tract j, and y_i is the unobserved population count for each grid i inside the tract j. The Poisson processes in each pixel are considered independent conditional on the underlying population latent surface. Thus, this sum also follows a Poisson distribution with mean equal to the sum of the means of each pixel Poisson process, that is,

$$Y_j \sim Poisson(\sum_{i=1}^{N_j} \lambda_i),\ j = 1, \dots, n_A \quad (14)$$

n_A is the number of tract population observations. Thus, we can compute the likelihood function of the model (hyper)parameters $\boldsymbol{\theta} = (\boldsymbol{\beta}, \sigma_\eta^2, \kappa, \sigma_\phi^2, \rho)$. The model was implemented in R using the Template Model Builder (TMB) package, and the parameters were estimated by maximizing the likelihood estimators (MLEs). A statistical review of the TMB package is elaborated in the following section.

3.3.1 Template Model Builder (TMB)

Disaggregation modeling is intrinsically different from prediction modeling as the interpolations and the observations are usually at a different scale. Traditionally, the spatial modeling software package integrated nested Laplace Approximation (INLA) (Rue et al., 2009) has been widely adopted to solve various spatial modeling circumstances. Nonetheless, it is only able to solve the spatial disaggregation problem when the link function in the latent field is linear (Wilson and Wakefield, 2018). Thus, for the HPSDRM proposed in this study which is a non-Gaussian generalized linear mixed model (NGLMM) with a log function as its link function in the latent field, the INLA package cannot achieve the goal of implementing the spatial disaggregation regression task.

Fortunately, the TMB (Kristensen et al., 2016) package offers more flexibility in modeling complex spatial problems based on C++. It integrates several powerful packages, including CppAD (Bell, 2012), for automatic differentiation in C++, Eigen (Guennebaud et al., 2010), for linear algebra in the C++ library, and CHOLMOD (Chen et al., 2008), for efficient computation of sparse matrices.

In this project, we created a C++ negative joint log-likelihood (NLL) objective function template in the format expected by TMB and calculate the joint likelihood and hyperpriors as a function of the model parameters and the spatial random effects. Then, the TMB package calculated estimates of both parameters and random effects' MMAP using the Laplace approximation for the marginal likelihood by evaluating the objective negative log-likelihood function and its derivatives through R's stats package nlminb function.

3.3.2 Bayesian inference of Matérn kernel covariance parameters using the Spatial Partial Differential Equation (SPDE) approach

The continuous Matérn field is internally difficult to interpret by traditional inference approaches. However, the Gaussian Random Markov Field (GMRF) stochastic partial differential equation (SPDE) is a great solution to this challenge (Lindgren et al., 2011).

$$(\kappa^2 - \Delta)^{\alpha/2}(\tau\xi(s)) = \omega(s) \quad (15)$$

where $s \in \mathbb{R}^d$, Δ is Laplacian, α is a smoothness parameter, $\kappa > 0$ is the scale parameter, τ controls the marginal variances of the Matérn covariance function, and $\omega(s)$ is a Gaussian spatial white noise process.

The exact solution of this linear fractional SPDE is verified to be the Gaussian random field $\boldsymbol{\eta}$ with the Matérn variance-covariance kernel (Lindgren et al., 2011, Blangiardo and

Cameletti, 2015). Thus, we can use the finite element method through a basis function representation to develop an approximation to the SPDE's exact solution. The basis function representation can be defined on a triangulation of the domain $\mathcal{D}$,

$$\xi(s) = \sum_{g=1}^{G} \varphi_g(s)\widetilde{\xi_g} \tag{16}$$

where G is the total number of vertices of the triangulation, $\{\varphi_g\}$ is the set of basis functions, and $\{\widetilde{\xi_g}\}$ are zero-mean Gaussian distributed weights.

Thus, for each linear predictor, we have

$$\eta_i = \boldsymbol{x}_i'\boldsymbol{\beta} + \sum_{g=1}^{G} \varphi_g(s_i)\widetilde{\xi_g} \tag{17}$$

where $\varphi_g(s_i)$ is the value of the gth basis function evaluated in the s_i grid point. The linear predictor is:

$$\eta_i = \boldsymbol{x}_i'\boldsymbol{\beta} + \sum_{g=1}^{G} A_{ig}\widetilde{\xi_g} \tag{18}$$

where $A_{ig} = \varphi_g(s_i)$ maps the GMRF $\widetilde{\xi_g}$ from the G triangulation vertices to the $n_{\mathcal{A}}$ observational locations (Blangiardo and Cameletti, 2015).

3.3.3 Scale function to preserve the pycnophylactic property

To preserve the pycnophylactic property of the dasymetric mapping process, a scale function (equ.19) is applied to the interpolated grids population so that the sum of the grid's population is equal to the original tract observations,

$$Pop_i = Pop_j \times \frac{p_i}{\sum_{i \in j}(p_i)} \tag{19}$$

where Pop_i is the estimated value in the grid i, Pop_j is the observed value in the tract j that the grid i resides in, and p_i is the predicted grids population output from the HPSDRM.

3.3.4 HPSDRM Model Setup

For the HPSDRM model application in the Nashville case study, weak informative hyperpriors were provided and summarized in Table 5. Specifically, we used the penalized complexity (PC) priors for the Matérn kernel's range and scale parameters, aiming to regularize the model towards a flatter field with a smaller magnitude (Fuglstad et al., 2019). These PC priors are determined to help avoid the problem of overfitting, simplifying the interpretation of the posterior results (Fuglstad et al., 2019). A negative joint log-likelihood objective function in the format expected by the C++ template was built based on the theories discussed above. Then, the tract population and selected land cover covariates were input into the model to conduct the Bayesian inferencing process. The mesh construction for solving the SPDE is provided in the supplemental material. The model-fitted results were inferenced by the joint-posterior approximated by the asymptotic Gaussian distribution with the mean of estimated MMAPs and the joint variance-covariance matrix calculated from the TMB. For all model parameters except the two Matérn kernel hyperparameters, random samples were drawn from the joint posteriors to compare with the priors.

One of the innovations of the HPSDRM model is that it provides uncertainty analysis for the prediction results since it is intrinsically a Bayesian inference model. Since each model's posterior sample maps to a prediction realization, uncertainties of the model prediction were inferenced by calculating the confidence interval at the 0.975 and 0.025 levels from the sampled prediction realizations. Detailed information regarding the HPSDRM model fitted results of the Nashville disaggregated grids population are presented in the Results section.

Table 5. Summary of the (hyper)priors used in the HPSDRM model application in the Nashville case study.

Parameter	Family	Prior parameters
Intercept	Gaussian	mean = 0, sd = 2
LC (DOS, DLI, DMI)	Gaussian	mean = 0, sd = 1
Range ($\boldsymbol{r}$)	PC	min = 1.5, prob = 0.01
Scale ($\boldsymbol{\sigma_\eta}$)	PC	max = 0.25, prob = 0.01
Logit (lambda) (logit ($\boldsymbol{\lambda}$))	Gaussian	mean = 0, sd = 15
Precision ($\boldsymbol{\frac{1}{\sigma_\phi^2}}$)	Gamma	shape = 1, scale = 2

4. RESULTS AND DISCUSSION

4.1 Social Fabric Index and its Uncertainty and Sensitivity Analysis: Nashville Case Study

Figure 4(d) presents the baseline index for the inductive SoFI model for tracts in Davidson County. Census tracts identified with better social cohesion status represent larger rankings of the baseline shown in dark blue colors, while smaller rankings of the baseline index signify worse social cohesion shown in red colors, with the remaining 30 percent of tracts assigned moderate social cohesion rankings shown in orange and yellow colors. A clear pattern is identified that social cohesion is generally better in rural communities rather than urban areas, echoing the findings from previous studies (Avery et al., 2021). Tracts with lower social cohesion are found to be clustered in the downtown area, which highly correlates with the low-income population density distribution pattern. Groupings of higher social cohesive census tracts are identified along the northwestern part of the county, where fewer crimes exist . These findings support our hypothesis that social cohesion is a strong indicator of social cohesive population and its associational relationship with places, where rural areas can take advantage of every social fabric dimension including sociodemographic diversity, physical infrastructure, green and public spaces and social engagement. Nonetheless, urban areas lack these elements to pursue a cohesive environment though they provide vitality to attract diverse population groups from different cultural backgrounds. Study found that although high density of neighborhood and land use mix might indicate a higher urban vitality, they might cause damage to social cohesion since strained relations, mass population migration movements, and possibly high crime rates could lead to social fragmentation (Mouratidis and Poortinga, 2020). This points out the importance of efficiently evaluating the effects of flood mitigation strategy like home buyouts on those inland waterway communities. Take the city of Nashville as an example, home buyouts usually occur to those downtown communities close to inland Cumberland River waterways after the 2010 flood. The buyouts could accelerate the population movement and migration, further worsening the social fabric status of these originally fragmentated communities.

The Monte Carlo simulation produced a distribution of the SoFI rankings for each tract, providing a means to evaluate uncertainty in the index rank model. Figure 4(a) presents the social fabric median ranking for each tract based on the simulation results, which we consider as a rough approximation to the 'true' index value. Comparing Figure 4(a) and (d), we identify similarities between baseline and median ranking for most tracts, suggesting that our baseline index can successfully capture the social fabric information of the area with adequate accuracy. Specifically, both indices illustrate the trend of a worse social cohesive status for those tracts around the downtown area and a better social fabric structure for those tracts along the northwestern rural communities of the county. However, some certain discrepancies can be found between the median and baseline index, especially for those small tracts in the heart of the county, where baseline rank identified those tracts as social fragmented areas, median rank seems to miscategorize these tracts into the social cohesive category since median value tends to enlarge the index rank. This stresses the importance of performing uncertainty analysis of the model. To better quantify and visualize the relationship between uncertainty and SoFI ranking associated with each tract, we used bivariate map to visualize the index ranking value and its descriptive uncertainty metrics in the same plot (Figure 4(b) - (c), (e) - (f)).

Here, we used transparency to present uncertainty metrics where alpha was set to 1 (fully opaque) to represent tracts with the lowest uncertainty, and alpha was set to 0 (fully transparent) to represent the largest uncertainty. Figure 4(b) and (c) are the spatial representation of the SoFI model uncertainty, showing that tracts with worse social fabric status tend to have a more extensive CV and a wider CI. Clear visualization of some missing tracts in both Figure 4(b) and (c) suggests that SoFI model is very uncertain about its judgment of the social fabric status of these tracts, including those tracts in the southeastern part of the county mentioned above. Compared with Figure 4(a), we found that SoFI model is better at determining moderate social fabric tracts than those with higher or lower social fabric status, especially for those tracts with a lower degree of social cohesion. The visualization of baseline rank bivariate map suggests similar findings (Figure 4(d) – (e)). Tracts with moderate social fabric status are opaquer than those with a higher or lower degree of social cohesion, supporting the conclusion from the median rank model.

Figure 5(a) and (c) reveal the relationship between median and baseline social fabric rank and index variability from CV perspectives, respectively. A negative correlation between social fabric rank and index variability is revealed that the index variability and uncertainty increase with the decrease of the social cohesion level. This relationship is also identified in Figure 4 and again verified by previous studies (Tate, 2013). The relationship between CI and social fabric rank shown in Figure 5(b) and (d) also exhibits a similar trend compared to CV results. The difference is that not only for weak social cohesive tracts, CI also suggests a larger uncertainty with the increase of social fabric index (Figure 5(b), (d)). As SoFI is aimed to identify social fragmented areas with lower social cohesion status, this indicates that the index model is better at filtering moderate social cohesive areas rather than identifying communities with higher or lower level of social fabric status. However, the SoFI model can serve as a guidance to capture the general trend of social fabric status from rural to urban communities.

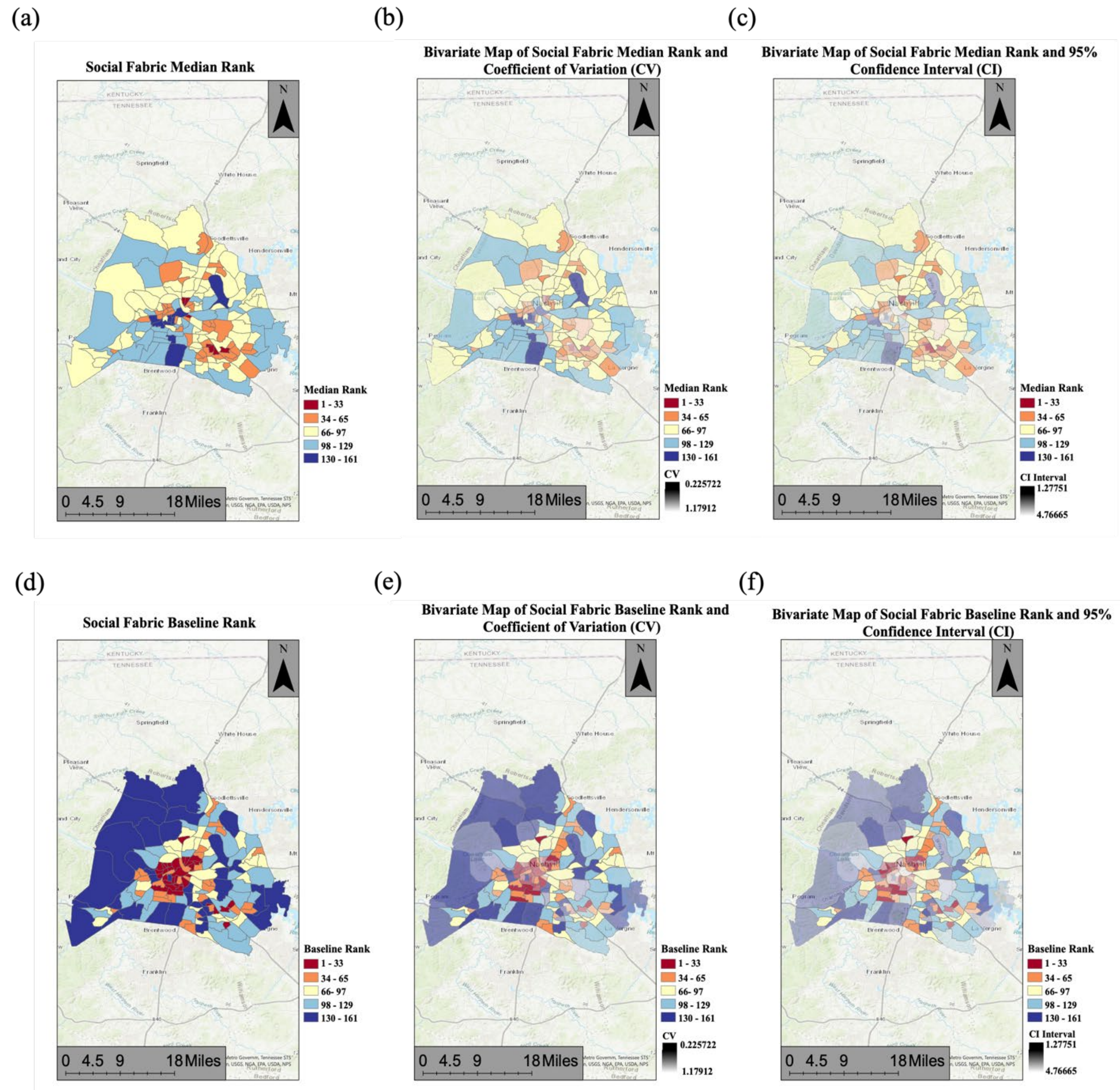

Figure 4. SoFI and its uncertainty visualizations: (a) SoFI median rank for tracts in the Davidson County; (b) SoFI median rank and CV for tracts; (c) SoFI median rank and 95% CI for tracts; (d) SoFI baseline rank for tracts; (e) SoFI baseline rank and CV for tracts; (f) SoFI baseline rank and 95% CI for tracts.

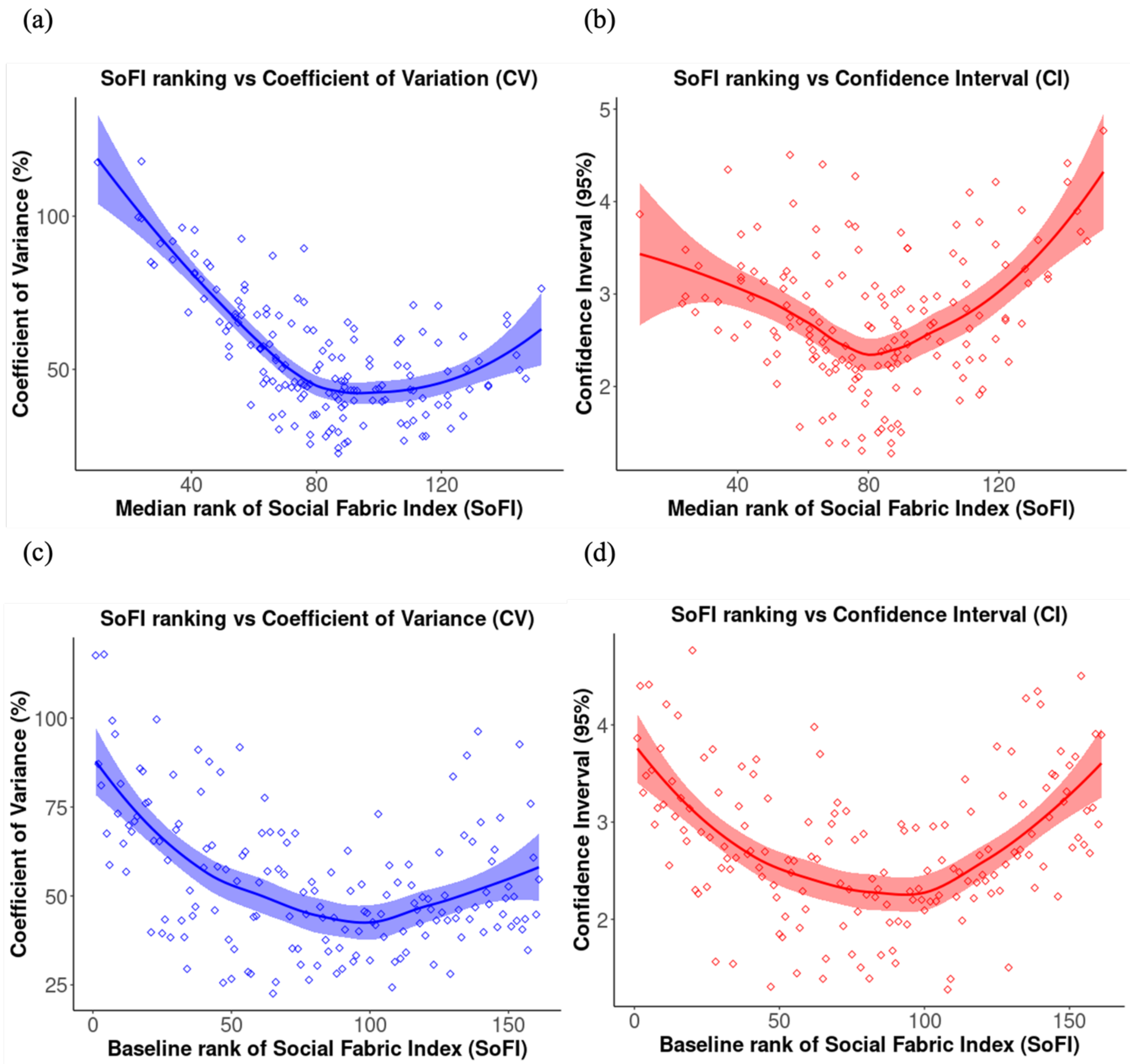

Figure 5. The relationship between SoFI rank and uncertainty descriptive metrics: (A) median rank with CV; (B) median rank with CI; (C) baseline rank with CV; (D) baseline rank with CI.

The median and variance are essential measurements to exhibit the reliability of the index model designs. However, the question of which model parameters are the main drivers of those uncertainties remains unknown. Global sensitivity analysis provides a diagnostic tool to produce sensitivity indices that can evaluate the behavior of model parameters in terms of both first-order and interactive total effects perspectives. The sensitivity indices for the model are shown in Table 6 and Figure 7. The first-order index values are vital to determine highly effective construction alternatives, and total-effect index values provide a comprehensive view of the total influences brought by each construction stage, including its own and interactions with others.

For this inductive SoFI model, the transformation and PCA selection are the two important construction parameters with high first-order and total-order effects of sensitivity indices (Figure

7). Taken together, the first-order effects account for 0.44 of the total variances, meaning that some degrees of interactions are involved between these parameters. We identified the most significant output variance contributor for each tract to map the dominating factors of SoFI ranking model for Davidson County (Figure 6). Figure 6 suggests that indicator transformation parameters tend to contribute more uncertainties to those tracts with higher or lower areas, while the weighting scheme plays more critical roles in those tracts with smaller sizes. PCA selection dominates uncertainty contributions for certain amounts of tracts since it highly correlates with the following rotation and weighting scheme stages, overriding some of the uncertainty contributions from the following construction steps. Thus, the roadmap to reducing the uncertainty in the SoFI is clear: focus more on choosing the appropriate transformation approach when the mapping units are highly heterogenous, and the combination of PCA selection, rotation and weighting scheme when mapping standard homogenous units that best represent model's principals.

Dominant Factors of Social Fabric Index (SoFI) Rank Model

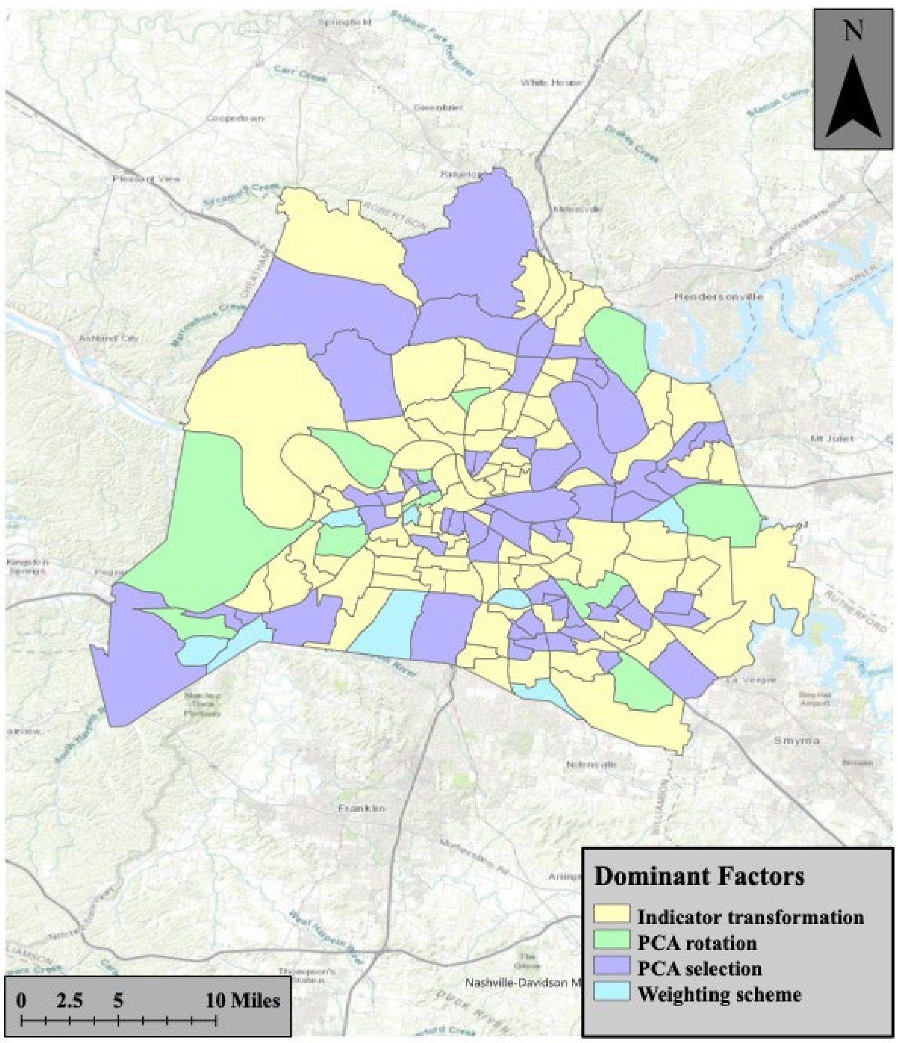

Figure 6. Identified dominating factors of SoFI ranking model for each tract of the Davidson County, Nashville.

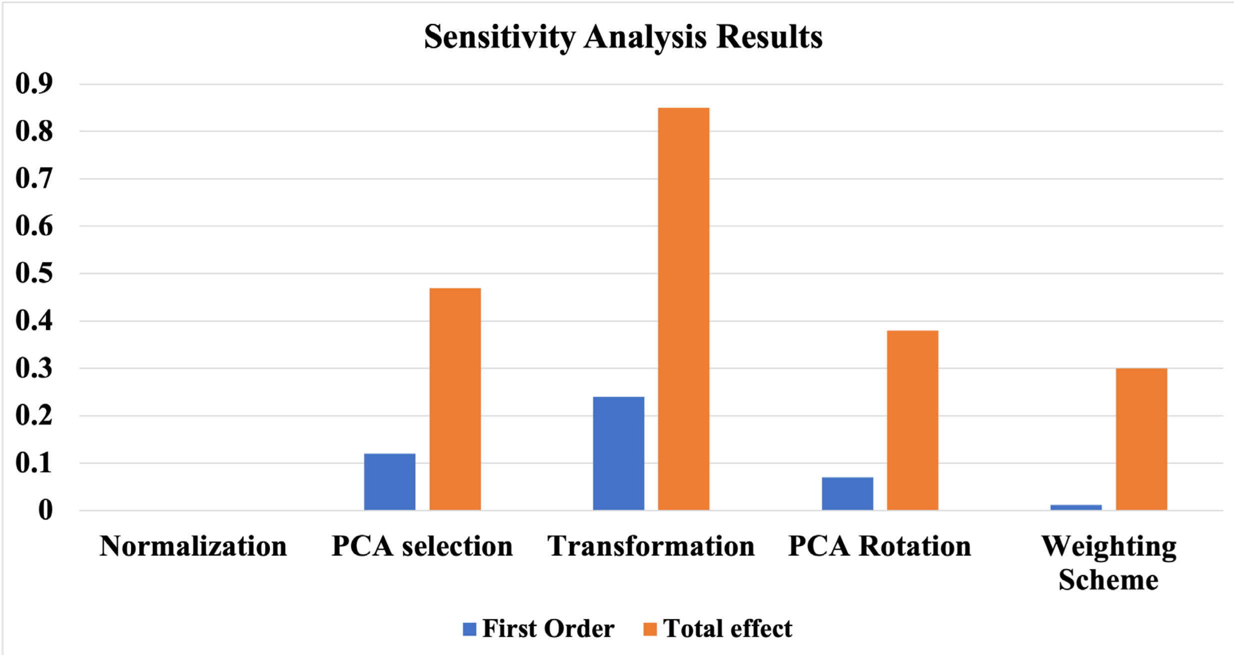

Figure 7. Sensitivity analysis Results.

Table 6. Summary of sensitivity analysis results.

Sensitivity Index/Construction Stage	Normalization	Transformation	PCA Selection	PCA Rotation	Weighting Scheme
First-order	0	0.24	0.12	0.07	0.012
Total effect	0	0.85	0.47	0.38	0.3

4.2 Dasymetric mapping: HPSDRM application in Nashville case study

The HPSDRM model input information is displayed in Figure 8. The polygon response data was obtained by the Decennial 2020 tract population, and the land cover predictors were retrieved by aggregating the NLCD 2019 land cover raster by a factor of 5 to produce the targe grids resolution of 150m * 150m. Thus, the range of each land cover predictor is [0, 25] since each target grid consists of a total of 25 original 30m * 30m grids (Figure 8(c.1) – (c.3)). Figure 8(b) shows the INLA mesh that required to solve the SPDE associated with the Matérn random field.

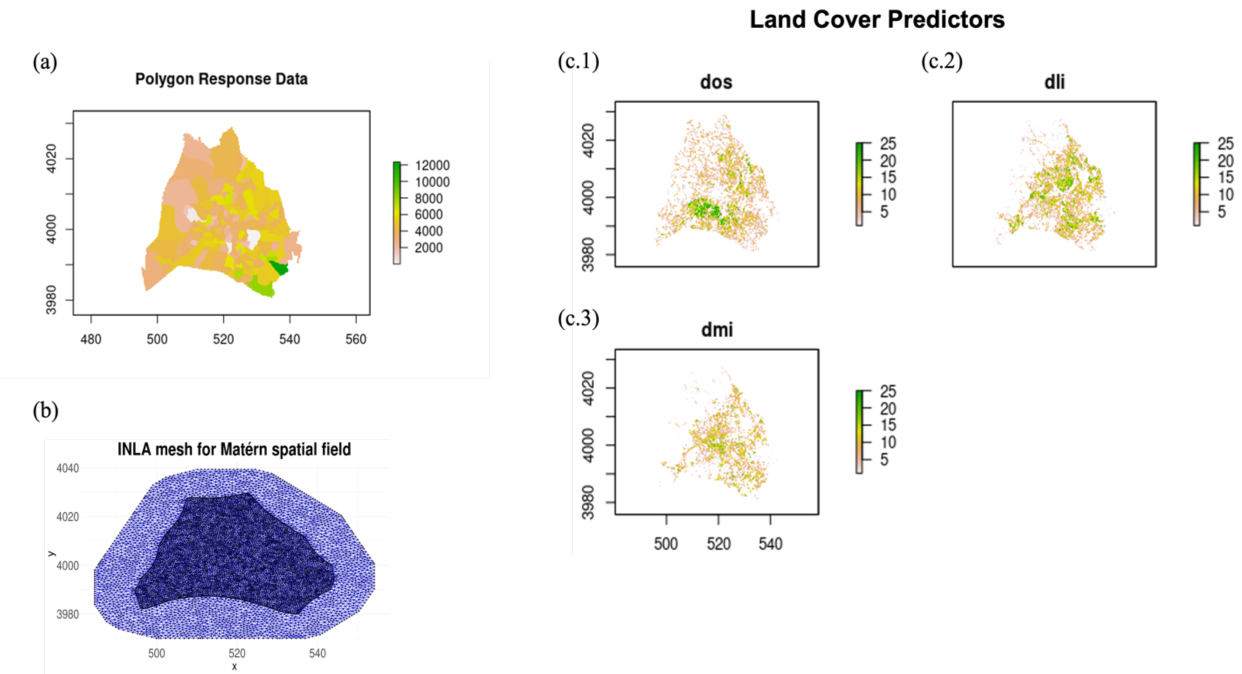

Figure 8. HPSDRM model input: (a) polygon response data is the tract population; (b) INLA mesh for solving SPDE of Matérn spatial field; (c.1) - (c.3) land cover predictors data.

The summary of the model-fitted results are presented in Figure 9. The MMAP estimates and standard error of the model's fixed effects, including the intercept, three land cover predictors, two hyperparameters for the Matérn field, and two hyperparameters for the CAR field are revealed in Figure 9(a). Figure 9(a) suggests that MMAP estimates for the hyperparameters of the random effects generally have more considerable uncertainties than the MMAP estimates for the land cover and the intercept coefficients. Figure 9(c.1) – (c.6) exhibit the priors and posterior samples drawn from the asymptotic normality posterior distribution for all the (hyper)parameters except the range and scale for the Matérn field. The red dotted vertical line is the MMAP estimate for the parameter (Figure 9(c.1 – (c.6)). All parameters' posterior samples were restricted well within the prior, indicating that the prior is noninformative enough without biasing the parameters' inferencing process. The model's out sample performance was evaluated by comparing the true block population and the predicted block population shown in Figure 9(b). The blue line is the $y = x$ and the black dots are the true and predicted population value for each block (Figure 9(b)). A clear positive correlation between the true and predictions suggests that the model successfully interpolated grids population in each tract with good accuracy.

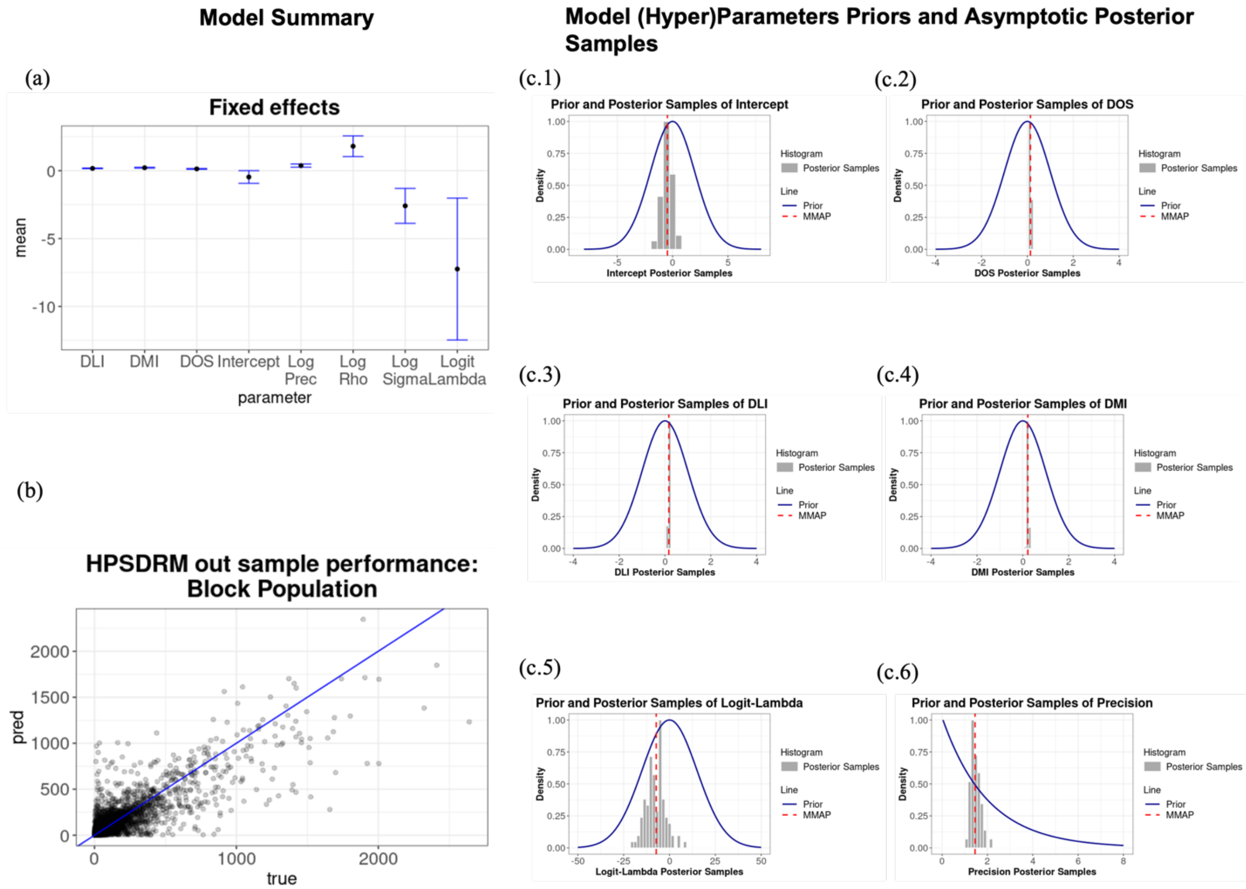

Figure 9. Summary of model fitting posteriors: (a) fixed effects parameters; (b) model out sample performance assessed by block population; (c) (hyper)parameters priors and asymptotic normality posterior samples.

Figure 10 presents the model prediction results and the decomposition of the latent surface contributions by the land cover covariates, the Matérn random field, and the CAR random field. Figure 10(a) suggests that for each tract, there are significant heterogeneities in population distribution, which cannot be revealed in Figure 10(a). The land cover covariates' contributions show similar trends as the grid's population prediction, explaining the most variances of the model's latent surface (Figure 10(b)). Additionally, the Matérn random field plays an essential role in incorporating the spatial autocorrelation pattern at the grid level, although the scale of the Matérn field is minor (Figure 10(c)). Figure 10(c) shows that the population tends to be similar and clustered in the downtown area and the southeastern part of Davidson County, supporting the distribution pattern revealed in Figure 8(a). Regarding the CAR random effects contributions, similar patterns can be identified that tracts surrounding the downtown area and the south part of the county force the population distribution to be similar. In conclusion, the areal level CAR spatial dependence and the grids level spatial autocorrelation are crucial in determining the finer grid population distribution characteristics.

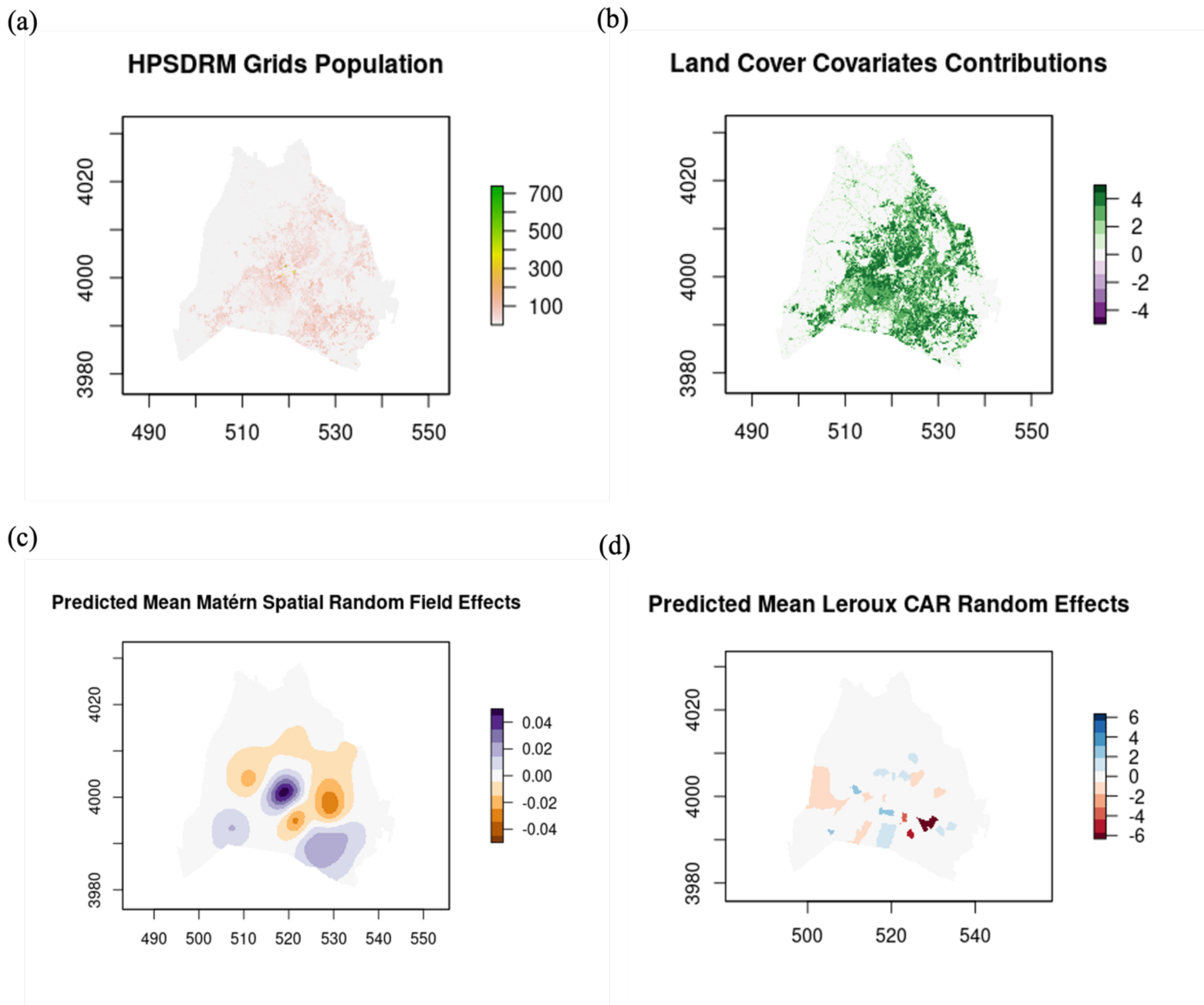

Figure 10. HPSDRM model mean prediction decompositions: (a) HPSDRM disaggregated grids mean population; (b) land cover covariates contributions to the model's latent surface; (c) Matérn random field mean contributions to the model's latent surface; (d) CAR random field mean contributions to the model's latent surface.

Finally, uncertainties predictions were computed based on the sampled prediction realizations shown in Figure 11. For each grid, confidence levels at 0.025 and 0.975 of the prediction realizations are shown in Figure 11(a), and four examples of prediction realizations are revealed in Figure 11(b.1) – (b.4). By comparing the two confidence levels predictions in Figure 11(a), areas with more prediction confidence and uncertainties can be easily identified. In this case, most areas have relatively small disaggregation prediction uncertainties (Figure 11(a)).

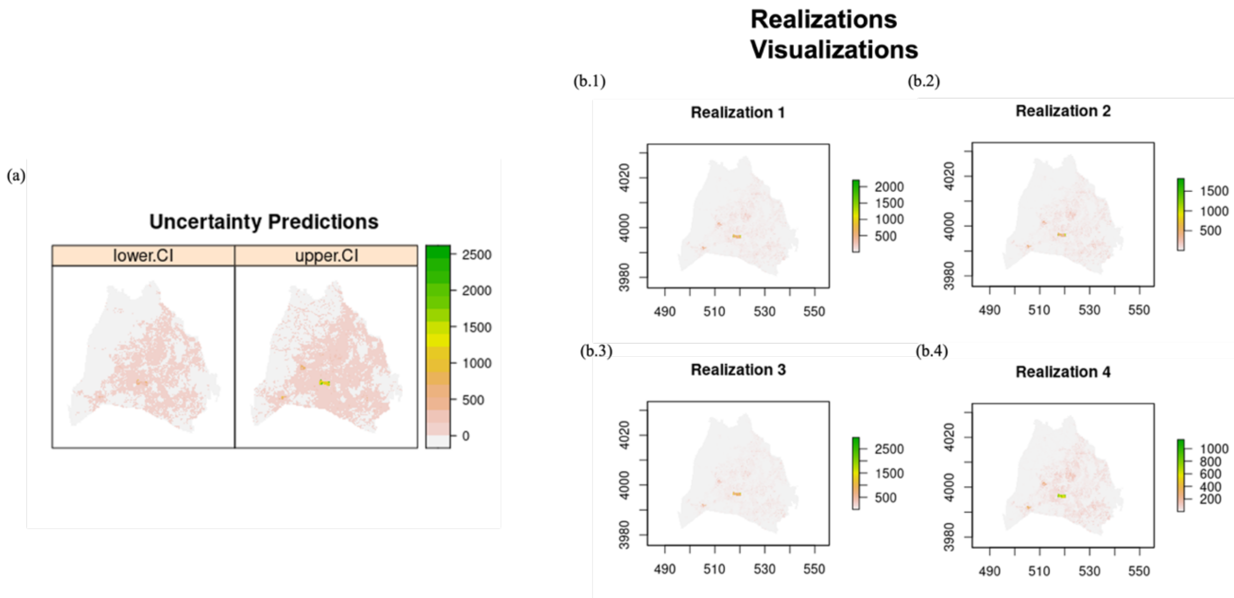

Figure 11. HPSDRM model uncertainty predictions: (a) confidence interval of model predictions; (b) visualization of 4 sampled prediction realizations.

5. IMPLICATIONS AND FUTURE CONSIDERATIONS

This project adopted an inductive model structure to incorporate a series of indicators related to real and behavioral aspects of the community social fabric concept to compute a quantitative social fabric index model (SoFI). Using this proposed model, we produced a census tract-level social fabric map of Davidson County, Nashville, a large inland river city as a case study. The interest was to better understand to what extent an extensive home buyout program to mitigate flood damages has impacted the social fabric of the community. The intent was to demonstrate the potential unintended social impacts of such programs on communities. While it is important to remove individuals from harm's way, it is just as important to consider the impacts of such actions on individuals and their connectedness to others and community assets/resources. Such practices are becoming more commonplace in riverine communities as we observe more intense flooding associated with climatic changes.

To validate the model's robustness for future applications and transferability, we utilized an internal validation path, using uncertainty analysis and global sensitivity analysis to systematically assess the construction alternatives associated with model configurations. A physical indicator-based social fabric index is a starting point to uncover the influences of hazard mitigation strategies like home buyouts on a community's social capital and cohesion, which has been overlooked by previous studies. We found that our proposed SoFI model presents a high-quality social fabric map highly correlated to the community's urban and rural characteristics. However, although the SoFI can provide valuable information of a community's social fabric status from a physical and behavior perspective, the emotional and psychological attachment to the places might be neglected by the current model. As such, the effects of the emotional and psychological indicators on the model remain unknown and should be investigated in future work.

The goal of this project also included applying the uncertainty and global sensitivity analysis to evaluate and visualize uncertainty for an inductive social fabric index model. We used a Monte Carlo simulation experiment to assess five sources of epistemic uncertainty: indicator normalization, indicator transformation, PCA selection, PCA rotation, and weighting scheme. Overall, the simulation results suggest a larger uncertainty in areas of a worse social fabric, indicating that proper use of the SoFI model as a screener to filter out the moderate and high social cohesive areas from the consideration, so further investigations can recognize those vulnerable social cohesive areas. Meanwhile, the global sensitivity analysis results indicate that only some stages of index construction process are important for model's output uncertainty. The indicator transformation and weighting scheme are the two crucial uncertainty contributors in all the construction stages. However, these two model parameters contribute differently under different circumstances. For instance, SoFI model focused on mapping social fabric status on a heterogenous scale might suffer less epistemic uncertainty from the weighting scheme stage than mapping on the standard homogeneous scale. Likewise, the transformation is not considered as an uncertainty factor for the SoFI model explicitly designed for application at a particular homogeneous spatial scale. Future work aims to validate this hypothesis by applying SoFI model to more case study areas with various community social characteristics.

The project also developed a geo-spatial disaggregation model to interpolate population for a more realistic distribution across the space. We proposed a hierarchical Poisson Spatial Disaggregation Regression Model (HPSDRM) to incorporate land cover covariates and spatial autocorrelation characterizations of two spatial scale levels. The proposed HPSDRM was applied to the Davidson County, Nashville, at the census tract level to disaggregate the tract population to finer grids population with a 150m x 150m resolution. The predicted grid population map successfully reveals the heterogeneity as well as hotspots and cold spots of the population distribution within the tracts. This suggests that spatial autocorrelation is indispensable in conducting the spatial disaggregation task. The proposed HPSDRM is expected to be readily applied to various disaggregation schemes, including other socioeconomic indicators of various composite index models.

In summary, this project has led to creation of both a SoFI and means to disaggregate census data to further investigate the potential impacts of programs such as buyouts on community vulnerabilities and in turn, potential resilience to inland waterway flooding. However, these models are only conceptual tools to advance the current flood mitigation strategy evaluation framework. The approaches could be applied to other areas with flooding to more wholistically consider the implications of mitigation strategies on vulnerable populations. Additional research could focus on applying the computational model and spatial disaggregation methods to investigate the effects of flood mitigation strategies like home buyouts on other communities along inland waterway and coastal areas. For example, the SoFI model and the HPSDRM could be utilized together to compare the pre-flood and post-flood social fabric status change at a localized level, especially for those communities with lower populations that may be more severely impacted with frequent flooding and where buyout programs may lead to decrease in population , connectedness, as well as the local tax base.

6. REFERENCES

Abramowitz, M. and Stegun, I. Handbook of mathematical functions. New York: Courier Dover Publications, 1972.

Abrash Walton, A., Marr, J., Cahillane, M. J., & Bush, K. (2021). Building Community Resilience to Disasters: A Review of Interventions to Improve and Measure Public Health Outcomes in the Northeastern United States. *Sustainability*, *13*(21), 11699.

Adger, W. N. (2000). Social and ecological resilience: Are they related? *Prog. Hum. Geogr.*, *24*(3), 347–364.

Adha, M. M., Budimansyah, D., Sapriya, S., & Sundawa, D. (2018). Enhancing Social Cohesion where Festival as a Media, is it Possible? *Advances in Social Science, Education and Humanities Research*, *251*, 213-217.

Ahlbrandt, R. (2013). Neighborhoods, people, and community. Springer Science & Business Media.

Alahmadi, M., Atkinson, P. M., & Martin, D. (2014). A comparison of small-area population estimation techniques using built-area and height data, Riyadh, Saudi Arabia. *IEEE Journal of Selected Topics in Applied Earth Observations and Remote Sensing*, *9*(5), 1959-1969.

Andrews, R. (2014). Coordinating for Cohesion: The Contribution of Public Management to the Cohesiveness of Society. *Public Performance & Management Review*, *37*(4), 705-721.

Anthoff, D., Nicholls, R. J., Tol, R. S., & Vafeidis, A. T. (2006). Global and regional exposure to large rises in sea-level: a sensitivity analysis.

Arup International Development. (2011). Characteristics of a safe and resilient community. International Federation of Red Cross and Red Crescent Societies, Geneva.

Avery, E. E., Hermsen, J. M., & Kuhl, D. C. (2021). Toward a better understanding of perceptions of neighborhood social cohesion in rural and urban places. Social Indicators Research, 157(2), 523-541.

Baker, C. K., Binder, S. B., Greer, A., Weir, P., & Gates, K. (2018). Integrating community concerns and recommendations into home buyout and relocation policy. *Risk, Hazards & Crisis in Public Policy*, *9*(4), 455-479.

Balica, S., & Wright, N. G. (2009). A network of knowledge on applying an indicator-based methodology for minimizing flood vulnerability. *Hydrological Processes: An International Journal*, *23*(20), 2983-2986.

Balica, S. F., Wright, N. G., & Van der Meulen, F. (2012). A flood vulnerability index for coastal cities and its use in assessing climate change impacts. *Natural hazards*, *64*(1), 73-105.

Baroni, G., & Tarantola, S. (2014). A General Probabilistic Framework for uncertainty and global sensitivity analysis of deterministic models: A hydrological case study. *Environmental Modelling & Software*, *51*, 26-34.

Beaujot, R. 2000. Earning and Caring in Canadian Families. Peterborough: Broadview

Bec, A., Char-lee, J. M., & Moyle, B. D. (2019). Community resilience to change: Development of an index. *Social Indicators Research*, *142*(3), 1103-1128.

Bell, BM. (2012). CppAD: A Package for C++ Algorithmic Differentiation. *Computational Infrastructure for Operations Research*, *57*, 10.

Blangiardo, M., & Cameletti, M. (2015). Spatial and spatio-temporal Bayesian models with R-INLA. John Wiley & Sons.

Bozheva, A. M., Petrov, A. N. and Sugumaran, R. (2005). The effect of spatial resolution of remotely sensed data in dasymetric mapping of residential areas. *GIScience and Remote Sensing*, *42*(2), 113–130.

Briggs, D. J., Gulliver, J., Fecht, D., & Vienneau, D. M. (2007). Dasymetric modelling of small-area population distribution using land cover and light emissions data. *Remote sensing of Environment*, *108*(4), 451-466.

Cannon, T., & Müller-Mahn, D. (2010). Vulnerability, resilience, and development discourses in context of climate change. *Natural hazards*, *55*(3), 621-635.

Cantle, T. (2001) Community Cohesion: A Report of the independent Review Team (London: Home Office)

Carpenter, A. (2013, October). Disaster resilience and the social fabric of space. In *Proceedings of the 9th International Space Syntax Symposium, Seoul, Korea* (Vol. 31).

CARRI, 2013. Building Resilience in America's Communities: Observations and Implications of the CRS Pilots. Community and Regional Resilience Institute. http://www.resilientus.org/wp-content/uploads/2013/05/CRS-Final-Report.pdf.

Carroll, J. B. (1953). Approximating simple structure in factor analysis. *Psychometrika*, *18*(1), 23–38.

Chakraborty, J., Maantay, J. A., & Brender, J. D. (2011). Disproportionate proximity to environmental health hazards: methods, models, and measurement. *American journal of public health*, *101*(S1), S27-S36.

Chang, H., & Franczyk, J. (2008). Climate change, land-use change, and floods: Toward an integrated assessment. *Geography Compass*, *2*(5), 1549-1579.

Chan, K., Tarantola, S., Saltelli, A. and Sobol', I. M. (2000). Variance based methods. In Sensitivity Analysis (eds A. Saltelli, K. Chan and M. Scott), pp. 167–197. New York: Wiley.

Chen Y, Davis TA, Hager WW, Rajamanickam S (2008). Algorithm 887: CHOLMOD, Supernodal Sparse Cholesky Factorization and Update/downdate. *ACM Transactions on Mathematical Software (TOMS)*, *35*(3), 22.

Clark, W. A. V., & Avery, K. L. (1976). The effects of data aggregation in statistical analysis. *Geographical Analysis*, *8*(4), 428–438.

Cockx, K., & Canters, F. (2015). Incorporating spatial non-stationarity to improve dasymetric mapping of population. *Applied Geography*, *63*, 220-230.

Collins, M., Chandler, R. E., Cox, P. M., Huthnance, J. M., Rougier, J., & Stephenson, D. B. (2012). Quantifying future climate change. *Nature Climate Change*, *2*(6), 403-409.

Corcoran, M. P., Gray, J., & Peillon, M. (2008). Ties that bind? The social fabric of daily life in new suburbs. In *Quality of Life in Ireland* (pp. 175-197). Springer, Dordrecht.

Cortes Jr, E. (1997). Reweaving the social fabric. *Families in Society*, *78*(2), 196-200.

Cox, J., House, D., & Lindell, M. (2013). Visualizing uncertainty in predicted hurricane tracks. *International Journal for Uncertainty Quantification*, *3*(2).

Cromley, R. G., Hanink, D. M., & Bentley, G. C. (2012). A quantile regression approach to areal interpolation. *Annals of the Association of American Geographers*, *102*(4), 763-777.

Cruz, I., Stahel, A., & Max-Neef, M. (2009). Towards a systemic development approach: Building on the Human-Scale Development paradigm. *Ecological economics*, *68*(7), 2021-2030.

Cui, K., & Han, Z. (2019). Cross-Cultural Adaptation and Validation of the 10-Item Conjoint Community Resiliency Assessment Measurement in a Community-Based Sample in Southwest China. *International Journal of Disaster Risk Science*, *10*(4), 439-448.

Cutter, S.L., Ash, K.D., and Emrich, C.T. (2014). The geographies of community disaster resilience. *Global Environmental Change, 29*, 65–77.

Cutter, S. L., Barnes, L., Berry, M., Burton, C., Evans, E., Tate, E., and Webb, J. (2008). A place-based model for understanding community resilience to natural disasters. *Global Environmental Change, 18*, 598–606.

Cutter, S. L., Boruff, B. J., & Shirley, W. L. (2003). Social vulnerability to environmental hazards. *Social science quarterly*, *84*(2), 242-261.

Cutter, S. L. (2016). The landscape of disaster resilience indicators in the USA. *Natural hazards*, *80*(2), 741-758.

Domínguez, M., & Montolio, D. (2021). Bolstering community ties as a mean of reducing crime. *Journal of Economic Behavior & Organization*, *191*, 916-945.

Ebisudani, M., and Tokai, A. (2017). The Application of Composite Indicators to Disaster Resilience: A Case Study in Osaka Prefecture, Japan. *Journal of Sustainable Development*, *10*, 81.

Ellis, C.D., A.H. Munnell, and A.D. Eschtruth. 2014. Falling Short: The Coming Retirement Crisis and What to Do about It Oxford University Press.

Eicher, C. L. and Brewer, C. A. (2001). Dasymetric Mapping and Areal Interpolation: Implementation and Evaluation. *Cartography and Geographic Information Science*, *28*(2), 125–138.

FEMA (Federal Emergency Management Agency). (2008). "HAZUS-MH: Preparedness and response planning." Washington, DC.

FEMA (Federal Emergency Management Agency). (2020). Michael Grimm Testimony to Committee on Science, Space and Technology. https://www.fema.gov/fact-sheet/michael-grimm-testimony-committee-science-space-and-technology (Accessed on Nov. 22/2022)

Ferguson, G. A. (1954). The concept of parsimony in factor analysis. *Psychometrika*, *19*(4), 281–291.

Firrantello, J., Bahnfleth, W. P., Musser, A., Freihaut, J. D., & Jeong, J. W. (2007). Use of factorial sensitivity analysis in multizone airflow model tuning. *ASHRAE Transactions*, *113*, 642.

Flanagan, B. E., Gregory, E. W., Hallisey, E. J., Heitgerd, J. L., & Lewis, B. (2011). A social vulnerability index for disaster management. *Journal of homeland security and emergency management*, *8*(1).

Flanagan, B. E., Hallisey, E. J., Adams, E., & Lavery, A. (2018). Measuring community vulnerability to natural and anthropogenic hazards: the Centers for Disease Control and Prevention's Social Vulnerability Index. *Journal of environmental health*, *80*(10), 34.

Ford, J. D., Pearce, T., McDowell, G., Berrang-Ford, L., Sayles, J. S., & Belfer, E. (2018). Vulnerability and its discontents: the past, present, and future of climate change vulnerability research. *Climatic Change*, *151*(2), 189-203.

Fraser, J., Elmore, R., Godschalk, D., Rohe, W. (2003) Implementing floodplain land acquisition programs in urban localities. The Center for Urban and Regional Studies, University of North Carolina at Chapel Hill, Chapel Hill, NC

Fuglstad, G. A., Simpson, D., Lindgren, F., & Rue, H. (2019). Constructing priors that penalize the complexity of Gaussian random fields. *Journal of the American Statistical Association*, *114*(525), 445-452.

Fukuyama, F. (1995). Trust: The social virtues and the creation of prosperity. New York: Free Press.

Gallent, N., A. Mace and M. Tewdwr-Jones (2003) Dispelling a myth? Second homes in Rural Wales. *Area, 35*(3), 271–284.

Gillespie-Marthaler, L., Nelson, K., Baroud, H., & Abkowitz, M. (2019). Selecting indicators for assessing community sustainable resilience. *Risk Analysis*, *39*(11), 2479-2498.

Giordano, A., & Cheever, L. (2010). Using dasymetric mapping to identify communities at risk from hazardous waste generation in San Antonio, Texas. *Urban Geography*, *31*(5), 623-647.

Guennebaud, G., Jacob, B., Avery, P., Bachrach, A., Barthelemy, S., et al. (2010). "Eigen V3."

Haasnoot, M., Kwadijk, J., Van Alphen, J., Le Bars, D., Van Den Hurk, B., Diermanse, F., ... & Mens, M. (2020). Adaptation to uncertain sea-level rise; how uncertainty in Antarctic mass-loss impacts the coastal adaptation strategy of the Netherlands. *Environmental Research Letters*, *15*(3), 034007.

He, B., and Ding, K. J. (2021). Localize the Impact of Global Greenhouse Gases Emissions under an Uncertain Future: A Case Study in Western Cape, South Africa. *Earth*, *2*(1), 111-123.

He, B., and Guan, Q. (2021). A Risk and Decision Analysis Framework to Evaluate Future $PM_{2.5}$ Risk: A Case Study in Los Angeles-Long Beach Metro Area. *International journal of environmental research and public health*, *18*(9), 4905.

Helton, J. C., Johnson, J. D., Oberkampf, W. L., & Sallaberry, C. J. (2010). Representation of analysis results involving aleatory and epistemic uncertainty. *International Journal of General Systems*, *39*(6), 605-646.

Hendrickson, A. E., & White, P.O. (1964). Promax: A quick method for rotation to orthogonal oblique structure. *British Journal of Statistical Psychology*, *17*(1), 65–70.

Heuser, B. L. (2005). Social cohesion and voluntary associations. *Peabody Journal of Education*, *80*(4), 16-29.

Hirschfield, A., & Bowers, K. J. (1997). The effect of social cohesion on levels of recorded crime in disadvantaged areas. *Urban Studies*, *34*(8), 1275-1295.

Holt, J. B., & Lu, H. (2011). Dasymetric mapping for population and sociodemographic data redistribution. *Urban remote sensing: Monitoring, synthesis, and modeling in the urban environment*, *250*, 195-210.

Homma, T. and Saltelli, A. (1996). Importance measures in global sensitivity analysis of model output. *Reliability Engineering and System Safety*, *52*(1), 1–17.

Horn, J. L. (1958). A rationale and test for the number of factors in factor analysis. *Psychometrika*, *30*(2), 179–185.

Hu, M., Wu, L., Xiang, G., & Zhong, S. (2021). Housing prices and the probability of marriage among the young: Evidence from land reform in China. *International Journal of Emerging Markets*, (ahead-of-print).

Iman, R. L., Johnson, M. E., & Watson Jr, C. C. (2005). Sensitivity analysis for computer model projections of hurricane losses. *Risk Analysis: An International Journal*, *25*(5), 1277-1297.

Jakeman, J., Eldred, M., & Xiu, D. (2010). Numerical approach for quantification of epistemic uncertainty. *Journal of Computational Physics*, *229*(12), 4648-4663.

Jansen, M. J. (1999). Analysis of variance designs for model output. *Computer Physics Communications*, *117*(1-2), 35-43.

Jia, P., & Gaughan, A. E. (2016). Dasymetric modeling: a hybrid approach using land cover and tax parcel data for mapping population in Alachua County, Florida. *Applied Geography*, *66*, 100-108.

Johansen, C., Horney, J., & Tien, I. (2017). Metrics for evaluating and improving community resilience. *Journal of Infrastructure Systems*, *23*(2), 04016032.

Kaiser, H. F. (1958). The varimax criterion for analytic rotation in factor analysis. *Psychometrika*, *23*(3), 187–200.

Kaiser, H. F. (1960). The application of electronic computers to factor analysis. *Educational and Psychological Measurement*, *20*(1), 141–151.

Kaly, U.L., Pratt, C.R., and Mitchell, J. (2014). The Environmental Vulnerability Index (EVI).

Kantzara, V. (2011). The relation of education to social cohesion. *Social cohesion and Development*, *6*(1), 37-50.

Kim, G. E., & Kim, E. J. (2020). Factors affecting the quality of life of single mothers compared to married mothers. *BMC psychiatry*, *20*(1), 1-10.

Kiureghian, A. D., and Ditlevsen, O. (2009). Aleatory or epistemic? Does it matter? *Structure Safety*, *31*(2), 105-12.

Kraan, C. M., Hino, M., Niemann, J., Siders, A. R., & Mach, K. J. (2021). Promoting equity in retreat through voluntary property buyout programs. *Journal of Environmental Studies and Sciences*, *11*(3), 481-492

Kristensen, K., Nielsen, A., Berg, CW., Skaug, H., Bell, BM. (2016). TMB: Automatic Differentiation and Laplace Approximation. *Journal of Statistical Software*, *70*(5), 1–21.

Kyllönen, M. (2019). A new narrative for the future: Learning, social cohesion and redefining "us". In Sustainability, human well-being, and the future of education (pp. 311-338). Palgrave Macmillan, Cham.

Langford, M. (2007). Rapid facilitation of dasymetric-based population interpolation by means of raster pixel maps. *Computers, Environment and Urban Systems*, *31*(1), 19-32.

Latham, A., & Layton, J. (2019). Social infrastructure and the public life of cities: Studying urban sociality and public spaces. *Geography Compass*, *13*(7), e12444.

Leaning, J., D. Guha-Sapir (2013). Natural disasters, armed conflict, and public health. *N. Engl. J. Med*, *369*, 1836–1842.

Lee, D. (2011). A comparison of conditional autoregressive models used in Bayesian disease mapping. *Spatial and spatio-temporal epidemiology*, *2*(2), 79-89.

Leroux, B. G., Lei, X., & Breslow, N. (2000). Estimation of disease rates in small areas: a new mixed model for spatial dependence. In Statistical models in epidemiology, the environment, and clinical trials (pp. 179-191). Springer, New York, NY.

Lindgren, F., Rue, H., & Lindström, J. (2011). An explicit link between Gaussian fields and Gaussian Markov random fields: the stochastic partial differential equation approach. *Journal of the Royal Statistical Society: Series B (Statistical Methodology)*, *73*(4), 423-498.

Lin, J., Cromley, R., & Zhang, C. (2011). Using geographically weighted regression to solve the areal interpolation problem. *Annals of GIS*, *17*(1), 1-14.

Li, T., & Corcoran, J. (2011). Testing dasymetric techniques to spatially disaggregate the regional population forecasts for Southeast Queensland. *Journal of Spatial Science*, *56*(2), 203-221.

Local Government Association (2002), Office of the Deputy Prime Minister, Commission for Racial Equality, The Inter-Faith Network, 'Guidance on Community Cohesion' London: LGA

Maantay, J. A., Maroko, A. R., & Herrmann, C. (2007). Mapping population distribution in the urban environment: The cadastral-based expert dasymetric system (CEDS). *Cartography and Geographic Information Science*, *34*(2), 77-102.

MacDonald, J., & Sampson, R. J. (2012). The world in a city: Immigration and America's changing social fabric. *The ANNALS of the American Academy of Political and Social Science*, *641*(1), 6-15.

Manzo, L. C., & Perkins, D. D. (2006). Finding common ground: The importance of place attachment to community participation and planning. *Journal of planning literature*, *20*(4), 335-350.

Matérn, B. Spatial variation. Berlin: Springer, 1986.

McGhee, D. J., Binder, S. B., & Albright, E. A. (2020). First, do no harm: evaluating the vulnerability reduction of post-disaster home buyout programs. *Natural Hazards Review*, *21*(1), 05019002.

Meerow, S., & Newell, J. P. (2019). Urban resilience for whom, what, when, where, and why? *Urban Geography*, *40*(3), 309-329.

Mennis, J and Hultgren, T. (2006). Intelligent dasymetric mapping and its application to areal interpolation. *Cartography and Geographic Information Science*, *33*(3), 179–194.

Mennis, J. (2009). Dasymetric mapping for small area population estimation. *Geography Compass, 3*, 727–745.

Mennis, Jeremy. (2003). Generating surface models of population using dasymetric mapping. *The Professional Geographer, 55*(1), 31-42.

Mennis, Jeremy. (2002). Using geographic information systems to create and analyze statistical surfaces of population and risk for environmental justice analysis. *Social science quarterly*, *83*(1), 281-297.

Messager, M. L., Ettinger, A. K., Murphy-Williams, M., & Levin, P. S. (2021). Fine-scale assessment of inequities in inland flood vulnerability. *Applied Geography*, 133, 102492.

Miller, B.J. 2016. Measuring Religion in Different patial Contexts: How Surveys Involving Religion Inconsistently Determine Locations. *Review of Religious Research*, *58*, 285-304.

Monteil, C., Simmons, P., & Hicks, A. (2020). Post-disaster recovery and sociocultural change: Rethinking social capital development for the new social fabric. *International Journal of Disaster Risk Reduction*, *42*, 101356.

Mouratidis, K., & Poortinga, W. (2020). Built environment, urban vitality and social cohesion: Do vibrant neighborhoods foster strong communities?. *Landscape and Urban Planning*, 204, 103951.

Nelson, K. S., Abkowitz, M. D., & Camp, J. V. (2015). A method for creating high resolution maps of social vulnerability in the context of environmental hazards. *Applied Geography*, *63*, 89-100.

Nelson, K. S., & Camp, J. (2020). Quantifying the benefits of home buyouts for mitigating flood damages. *Anthropocene*, *31*, 100246.

Neuhaus, W. (1954). The quartimax method: An analytical approach to orthogonal simple structure. *British Journal of Statistical Psychology*, *7*(2), 81–91.

Nickols, S. Y., Collier, B. J., & Holland, J. M. (2015). Families in the social fabric: unraveling or reweaving? Considerations for family and consumer sciences. *Journal of Family & Consumer Sciences*, *107*(1), 10-18.

Norris, F.H., Stevens, S.P., Pfefferbaum, B., Wyche, K.F., and Pfefferbaum, R.L. (2008). Community Resilience as a Metaphor, Theory, Set of Capacities, and Strategy for Disaster Readiness. *American Journal of Community Psychology, 41*, 127–150.

OSSPAC (Oregon Seismic Safety Policy Advisory Commission). (2013). "The Oregon resilience plan." Salem, OR.

Pendall, R., Foster, K.A., and Cowell, M. (2010). Resilience and regions: building understanding of the metaphor. *Cambridge J Regions Econ Soc, 3*, 71–84.

Petrov, A. (2012). One hundred years of dasymetric mapping: back to the origin. *The Cartographic Journal*, *49*(3), 256-264.

Pfefferbaum, R. L., Pfefferbaum, B., Van Horn, R. L., Klomp, R. W., Norris, F. H., & Reissman, D. B. (2013). The communities advancing resilience toolkit (CART): An intervention to build community resilience to disasters. *Journal of public health management and practice*, *19*(3), 250-258.

Pfefferbaum, R. L., Pfefferbaum, B., Nitiéma, P., Houston, J. B., and Van Horn, R. L. (2015). Assessing Community Resilience: An Application of the Expanded CART Survey Instrument with Affiliated Volunteer Responders. *American Behavioral Scientist*, *59*, 181–199.

Pianosi, F., Beven, K., Freer, J., Hall, J. W., Rougier, J., Stephenson, D. B., & Wagener, T. (2016). Sensitivity analysis of environmental models: A systematic review with practical workflow. *Environmental Modelling & Software*, *79*, 214-232.

Plyer, A., Ortiz, E., Horwitz, B., and Hobor, G. (2013). "The New Orleans index at eight." Greater New Orleans Community Data Center, New Orleans.

Rue, H., Martino, S., & Chopin, N. (2009). Approximate Bayesian inference for latent Gaussian models by using integrated nested Laplace approximations. *Journal of the royal statistical society: Series b (statistical methodology)*, *71*(2), 319-392.

Putnam, R. D. (2007). E pluribus unum: diversity and community in the twenty-first century the 2006 Johan Skytte prize lecture. *Scand. Polit. Stud*, *30*(*2)*, 137–174.

Puy, A., Becker, W., Piano, S. L., & Saltelli, A. (2020). The battle of total-order sensitivity estimators. arXiv preprint arXiv:2009.01147.

Puy, A., Piano, S. L., Saltelli, A., & Levin, S. A. (2021). sensobol: a R package to compute variance-based sensitivity indices. arXiv preprint arXiv:2101.10103.

Ravanera, Z. (2000, May). Family Transformation and Social Cohesion: Project Overview and Integrative Framework. In A revised version of Ravanera, ZR, and F. Rajulton, Multiple levels of analysis: Prospects and challenges for the family transformation and social cohesion project, a paper presented at the annual meeting of the Canadian Population Society in Edmonton, Alberta.

Saisana, M., Saltelli, A., & Tarantola, S. (2005). Uncertainty and sensitivity analysis techniques as tools for the quality assessment of composite indicators. *Journal of the Royal Statistical Society: Series A (Statistics in Society)*, *168*(2), 307-323.

Saltelli, A., Annoni, P., Azzini, I., Campolongo, F., Ratto, M., Tarantola, S. (2010). Variance based sensitivity analysis of model output. Design and estimator for the total sensitivity index. *Computer Physics Communications*, *181*(2), 259-270.

Saltelli, A., Tarantola, S. and Campolongo, F. (2000). Sensitivity analysis as an ingredient of modelling. *Statist. Sci*., *15*, 377–395.

Saltelli, A., Tarantola, S., Campolongo, F. and Ratto, M. (2004). Sensitivity Analysis in Practice, a Guide to Assessing Scientific Models. New York: Wiley.

Sampson, R. J., Raudenbush, S. W., & Earls, F. (1997). Neighborhoods and violent crime: A multilevel study of collective efficacy. *Science*, *277*(5328), 918-924.

Saunders, D. R. (1953). An analytical method for rotation to orthogonal simple structure (Research Bulletin 53–10). Princeton, NJ: Educational Testing Service.

Scawthorn, C., N. Blais, H. Seligson, E. Tate, et al. (2006). HAZUS-MS Flood Loss Estimation Methodoogy. I. Overview and Flood Hazard Characterization. *Natural Hazards Review*, 7(2).

Schmidtlein, M. C., Deutsch, R. C., Piegorsch, W. W., & Cutter, S. L. (2008). A sensitivity analysis of the social vulnerability index. *Risk Analysis: An International Journal*, *28*(4), 1099-1114.

Sempier, T. T., Swann, D. L., Emmer, R., Sempier, S. H., and Schneider, M. (2010). "Coastal community resilience index: A community self-assessment." MASGP-08-014, Ocean Springs, MS.

Shaw, R., Takeuchi, Y., Joerin, J., Fernandez, G., Tjandradewi, B., Chosadilla, Wataya, E., McDonald, B., Fukui, R., Sharma, A., et al. (2010). Climate and disaster resilience initiative capacity-building program - UNISDR.

Sherrieb, K., Norris, F. H., & Galea, S. (2010). Measuring capacities for community resilience. *Social indicators research*, *99*(2), 227-247.

Shim, J. H., & Kim, C. I. (2015). Measuring resilience to natural hazards: towards sustainable hazard mitigation. *Sustainability*, *7*(10), 14153-14185.

Sobol', I. Y. M. (1967). On the distribution of points in a cube and the approximate evaluation of integrals. *Zhurnal Vychislitel'noi Matematiki i Matematicheskoi Fiziki*, *7*(4), 784-802.

State & County QuickFacts (2020). United States Census Bureau. https://www.census.gov/quickfacts/fact/table/davidsoncountytennessee,TN,US/PST045221 (Accessed on Dec. 10/2022)

Stephenson, D. B., & Dolas-Reyes, F. J. (2000). Statistical methods for interpreting Monte Carlo ensemble forecasts. *Tellus A: Dynamic Meteorology and Oceanography*, *52*(3), 300-322.

Stevens, F. R., Gaughan, A. E., Linard, C., & Tatem, A. J. (2015). Disaggregating census data for population mapping using random forests with remotely sensed and ancillary data. *PloS one*, *10*(2), e0107042.

Su, M. D., Lin, M. C., Hsieh, H. I., Tsai, B. W., & Lin, C. H. (2010). Multi-layer multi-class dasymetric mapping to estimate population distribution. *Science of the Total Environment*, *408*(20), 4807-4816.

Tanner, W., O'Shaughnessy, J., Krasniqi, F., & Blagden, J. (2020). The State of our Social Fabric: Measuring the changing nature of community over time and geography.

Tapia, C., Abajo, B., Feliu, E., Mendizabal, M., Martinez, J.A., Fernández, J.G., Laburu, T., and Lejarazu, A. (2017). Profiling urban vulnerabilities to climate change: An indicator-based vulnerability assessment for European cities. *Ecological Indicators, 78*, 142–155.

Tate, E. (2012). Social vulnerability indices: a comparative assessment using uncertainty and sensitivity analysis. *Natural Hazards*, *63*(2), 325-347.

Tate, E. (2013). Uncertainty analysis for a social vulnerability index. *Annals of the association of American geographers*, *103*(3), 526-543.

UNDP (2016). Human Development Index (HDI) | Human Development Reports.

Utazi, C.E., Thorley, J., Alegana, V.A., Ferrari, M.J., Nilsen, K., Takahashi, S., Metcalf, C.J.E., Lessler, J. and Tatem, A.J. (2019). A spatial regression model for the disaggregation of areal unit based data to high-resolution grids with application to vaccination coverage mapping. *Statistical Methods in Medical Research*, *28*(10 -11), 3226-3241.

Van der Meer, T., and Tolsma, J. (2014). Ethnic diversity and its effects on social cohesion. *Annu. Rev. Sociol. 40*, 459–478.

Van Griensven, A., Francos, A., & Bauwens, W. (2002). Sensitivity analysis and auto-calibration of an integral dynamic model for river water quality. *Water Science and Technology*, *45*(9), 325-332.

Vita, G.E.D., Iavarone, R., Gravagnuolo, A., and Alberico, I. (2018). An Evaluation Framework

Western, J., Stimson, R., Baum, S., & Van Gellecum, Y. (2005). Measuring community strength and social capital. *Regional Studies*, *39*(8), 1095–1109.

Wilson, K., Wakefield, J. (2018). “Pointless Spatial Modelling.” Biostatistics.

Wobus, C., Porter, J., Lorie, M., Martinich, J., & Bash, R. (2021). Climate change, riverine flood risk and adaptation for the conterminous United States. *Environmental Research Letters*, 16(9), 094034.

Woolley, F. (2016). Social cohesion and voluntary activity: making connections. In *The economic implications of social cohesion* (pp. 150-182). University of Toronto Press.

Wrenn, D. H., Yi, J., & Zhang, B. (2019). House prices and marriage entry in China. *Regional Science and Urban Economics*, *74*, 118-130.

Wu, S. S., Qiu, X. and Wang, L. (2005). Population estimation methods in GIS and remote sensing: a review. *GIScience and Remote Sensing, 42*(1), 80–96.

Yoon, D.K., Kang, J.E., and Brody, S.D. (2016). A measurement of community disaster resilience in Korea. *Journal of Environmental Planning and Management, 59*, 436–460.

Yuliastuti, N. (2018). Utilization of social facilities to reinforce social interaction in formal housing.

Zahda, N., & Fukukawa, Y. (2008). Analyzing the social fabric in rehabilitated residential quarters the case of rehabilitated multi-family courthouses in old city of hebron. *Journal of Asian Architecture and Building Engineering*, *7*(2), 279-283.

Zandbergen, P. A. (2011). Dasymetric mapping using high resolution address point datasets. *Transactions in GIS*, *15*, 5-27.

Zavar, E. (2015). Residential perspectives: the value of Floodplain-buyout open space. *Geogr Rev, 105*(1): 78–95.

Zhang, Hansong, Joshua N. Hook, Jennifer E. Farrell, David K. Mosher, Laura E. Captari, Steven P. Coomes, Daryl R. Van Tongeren, and Don E. Davis. Exploring social belonging and meaning in religious groups. (2019). *Journal of Psychology and Theology, 47*(1), 3-19.

Zhou, Y., Smith, S. J., Elvidge, C. D., Zhao, K., Thomson, A., & Imhoff, M. (2014). A cluster-based method to map urban area from DMSP/OLS nightlights. *Remote Sensing of Environment*, *147*, 173-185.